J. Fluid Mech. (1993), *vol.* 248, *pp.* 605–635

Viscous flow normal to a flat plate at moderate Reynolds numbers

By S. C. R. DENNIS[1], WANG QIANG[1], M. COUTANCEAU[2] AND J.-L. LAUNAY[2]

[1] Department of Applied Mathematics, University of Western Ontario, London, Ontario, Canada

[2] Laboratoire de Mécanique des Fluides, Université de Poitiers, Poitiers, France

(Received 1 August 1989 and in revised form 29 June 1992)

An experimental and numerical investigation of the two-dimensional flow normal to a flat plate is described. In the experiments, the plate is started impulsively from rest in a channel for Reynolds numbers, based on the breadth of the plate, in the range $5 \leqslant Re \leqslant 20$. Over this range of Re the flow remains symmetrical and stable and tends to a steady state but is shown to depend strongly on the ratio λ of the plate to channel breadth. The evolution of the experimental flow with time and Reynolds number is studied and the variation with λ in the range $0.05 \leqslant \lambda \leqslant 0.2$ is investigated sufficiently to enable an estimate of properties of the flow as $\lambda \to 0$ to be obtained for the steady-state flow. The numerical results are obtained for steady flow normal to a flat plate in an unbounded fluid for Reynolds numbers up to $Re = 100$. They supplement and extend results for this flow obtained for values of Re up to 20 by Hudson & Dennis (1985). The present solutions have been found using a vorticity-stream function formulation rather than the primitive-variable approach of Hudson & Dennis and provide an independent check on these results. A comparison of the theoretical results for $Re \leqslant 20$ with the limit $\lambda \to 0$ of the experimental results is, generally speaking, extremely satisfactory.

1. Introduction

A paper by Hudson & Dennis (1985) has given results of calculations of the steady two-dimensional viscous flow of an incompressible fluid normal to an infinite flat plate of finite breadth in an unbounded fluid and made comparisons with some features of the existing experimental results of Prandtl & Tietjens (1934), Taneda (1968), Acrivos *et al.* (1968) and with a theoretical model of Smith (1979). The calculations were carried out using a solution procedure in terms of the primitive variables (velocity components and pressure) based on a method due to Belotserkovskii, Gushchin & Shchennikov (1975) which has certain advantages in the present problem in that the effect of the singularity in the vorticity at the edges of the plate does not directly enter the calculations. Solutions were obtained in the Reynolds-number range $0.1 \leqslant Re \leqslant 20$, where $Re = 2Ul/\nu$, $(l = \frac{1}{2}D)$, D being the plate breadth, U the velocity of the uniform stream at large distances and ν the coefficient of kinematic viscosity of the fluid (see figure 1). Over this range of Re the comparison between the numerical and experimental results was generally satisfactory. However, although the dependence on Re of the length of the separated region behind the plate was approximately linear, the gradient of the line was not in agreement with the theory of Smith (1979).

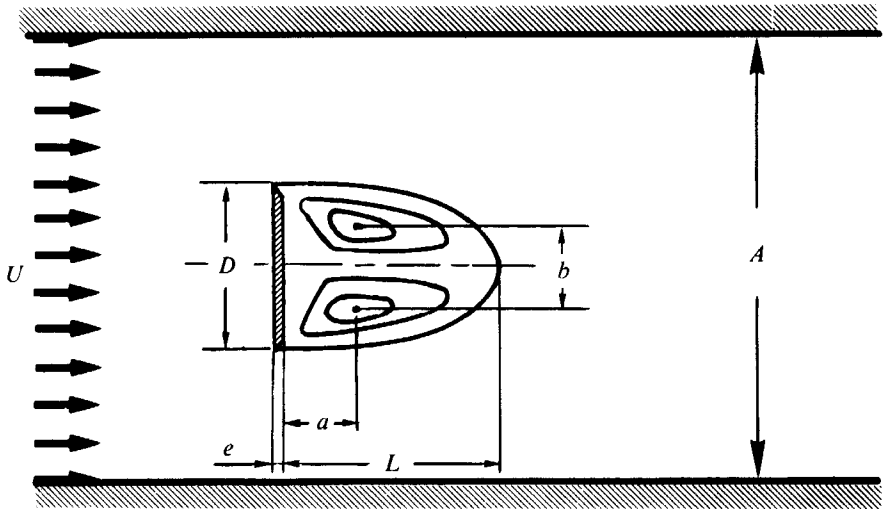

FIGURE 1. Geometrical parameters of the closed wake.

A more recent paper by Ingham, Tang & Morton (1990) has described a study of steady two-dimensional flow normal to an infinite array of plates, each of infinite length and finite breadth, whose planes lie in a single plane such that the edges of adjacent plates are parallel. The edges of each pair of adjacent plates are separated by the same constant gap, giving the flow a periodic structure. The problem was considered both theoretically and experimentally and the results of calculations were found to be in good agreement not only with the experiments but also with theoretical work on a related problem by Smith (1985). In fact, the theoretical work of Smith (1985) gives $L/D \sim 0.10\,Re$ for the ratio of the eddy length L to the breadth D of the plate, whereas Ingham *et al.* (1990) suggest $L/D \sim 0.105\,Re$ for large enough Re in their calculations, which cover the range $0 \leqslant Re \leqslant 500$. Moreover, an examination of their results indicates that this formula fits some values of L/D for quite low Re (e.g. $L/D = 1.054$ at $Re = 10$), whereas the calculations of Hudson & Dennis (1985) give substantially greater values of L/D. A possible reason is that a blockage effect exists in the flow normal to any individual plate in the case of the array, owing to the presence of the neighbouring plates. In the calculations of Hudson & Dennis, corresponding to a plate in an infinite field, there is no blockage ratio.

The present work is motivated by several objects. In the first place it is of importance to verify that the precise details of the calculated results correspond to those obtained in a comparable experimental study. An experimental study must necessarily be carried out in a channel of finite breadth in which the blockage ratio $\lambda = D/A$ (see figure 1) exerts an influence on the flow. No systematic study of this effect has previously been made. In the present paper we describe an experimental investigation of this effect on the flow normal to a flat plate started impulsively from rest in a channel. The range of Reynolds numbers is $5 \leqslant Re \leqslant 20$, over which the flow remains stable and attached and ultimately tends to a steady state. The limit of the steady-state results as the blockage ratio $\lambda \to 0$ is estimated and compared with the calculations of Hudson & Dennis (1985), which are themselves confirmed by some new calculations using the vorticity–stream function formulation of the Navier–Stokes equations.

The new calculations provide some results not given by Hudson & Dennis, for example the steady-state velocity profiles on the axis of symmetry fore and aft of the plate. The profiles aft of the plate can be compared with good precision with the limit as $\lambda \to 0$ of the corresponding experimentally measured profiles in the wake. The calculations are also extended for values of Re up to 100, well beyond the range covered by Hudson & Dennis and of the present experiments. There is motivation for this in view of the theoretical work of Smith (1979, 1985), Peregrine (1985) and the numerical work of Fornberg (1980, 1985). For example, Peregrine's discussion of Fornberg's calculations, which are for flow past a circular cylinder, points out that over a considerable range of Reynolds numbers Re the length of wake is proportional to Re and its breadth proportional to $Re^{\frac{1}{2}}$ consistently with Smith's (1979) model, but for higher Reynolds numbers the situation changes and, in particular, the breadth of the wake increases proportionately to Re. We can at least confirm from the present calculations for Re up to 100 that the properties of the wake in the case of a flat plate are also consistent with Smith's model and Fornberg's calculations. These are key properties of the flow at moderate Reynolds numbers; they are discussed later.

The experimental study is based on a technique of visualization which yields quasi-instantaneous velocity fields. Coutanceau & Bouard (1977*a*, *b*) have shown, in studying the development of the wake in the rear of a circular cylinder, that the effect of the confinement of the cylinder is an important factor, particularly for small Reynolds numbers. Unlike the case of the circular cylinder, little data exists in the literature concerning the experimental study of the wake development at the rear of a plate situated at right angles to the mainstream, particularly for small Reynolds numbers for which the wake remains attached to the plate. The existing ones are based on techniques of visualization, although the investigation of Acrivos *et al.* (1968) depends also on measurements of pressure, velocity and local shear stress. These authors demonstrated the similarity of the evolution of the steady-wake bubble as a function of Reynolds number for different forms of obstacles, of which the flat plate at right angles to the stream was considered for Reynolds numbers up to 200. Some geometrical characteristics of the re-circulating zone were given, such as the coefficient of proportionality between the length of the wake and the Reynolds number, the maximum width and the position of the centres of the vortices relative to it, but the study is mainly for $Re > 30$. The higher Reynolds numbers were realized by stabilizing the wake using a splitter plate placed at some distance from the obstacle and the value of λ was kept fixed at $\lambda = 0.05$. The flow was considered to be separated from the edges of the plate for all $Re > 0$.

Taneda (1968) analysed the steady-state flow for $0.1 \leqslant Re \leqslant 30$ and for a constant value $\lambda = 0.0325$, judged to be sufficiently small for the effect of the walls to be negligible. He gives details of the recirculating zone, such as its length and the position of the centres of the vortices, noting also the values $Re = 0.4$ and 25, respectively, at which the wake first appears and at which it starts to oscillate. Arakaki (1968) studied the different regimes in the evolution of the wake as a function of Reynolds number over the range $10 \leqslant Re \leqslant 100$ and gave values of the critical Reynolds numbers which separate them. He also found $Re = 25$ to be the Reynolds number at which the wake first started to oscillate. Plates of different breadths were used to obtain the range of Reynolds numbers investigated, but the value $\lambda = 0.1$ was maintained for all measurements using parallel plates as movable sidewalls. Results were also given for the development of the wake with time, but only for $Re \geqslant 80$. Finally, Taneda & Honji (1971) studied the development with time of the separated flow normal to a flat plate which was started from rest either

impulsively or with a uniform acceleration and with $\lambda = 0.026$. Amongst numerous visualizations, they have given the evolution of the wake length normalized in different fashions for a range of about $18 \leqslant Re \leqslant 1135$.

In none of these experimental investigations has a study of the effect of change in blockage ratio on the flow been made, so that it could be argued that none of the results can safely be compared with calculations of the flow in an infinite domain. In the present work the variation with λ of key flow properties such as the length and breadth of the separated wake and the position of the vortex centres is made. The effect of variation of λ on the flow is found to be of considerable importance but when the steady-state results are extrapolated to $\lambda = 0$ there is good agreement with the corresponding results of both the present calculations and those of Hudson & Dennis (1985). We thus have succeeded in linking both sets of calculations with the experiments for low values of Re and the present calculations with theoretical results for higher Re up to $Re = 100$, making a contribution to the understanding of the flow at least for moderate Re.

2. Basic theoretical equations and method of solution

The equations to be solved are the usual Navier–Stokes equations for the steady motion of an incompressible fluid past a flat plate occupying the position $x = 0$, $-l \leqslant y \leqslant l$ of Cartesian coordinates (x, y). The boundary conditions are that $u = v = 0$ on the plate and $u \to U$, $v \to 0$ as $x^2 + y^2 \to \infty$, where (u, v) are Cartesian velocity components and U is the free-stream velocity. Since the flow is symmetrical about the axis $y = 0$, it is necessary to consider only the flow in the half-plane $0 \leqslant y \leqslant \infty$.

Hudson & Dennis (1985) used an unsteady model of the flow in terms of u, v and the pressure p. The transformation of elliptic coordinates

$$x = l \sinh \xi \cos \eta, \quad y = l \cosh \xi \sin \eta, \tag{1}$$

was used to transform the problem to a more suitable domain. Here we shall use the same transformation but work in terms of a dimensionless stream function ψ and vorticity ζ which are defined by means of the equations

$$u = \frac{Ul}{\partial y}\frac{\partial \psi}{\partial y}, \quad v = -\frac{Ul}{\partial x}\frac{\partial \psi}{\partial x}, \quad \zeta = (l/U)\left(\frac{\partial v}{\partial x} - \frac{\partial u}{\partial y}\right). \tag{2}$$

The governing equations for ψ, ζ in the (ξ, η)-plane are then

$$\frac{\partial^2 \psi}{\partial \xi^2} + \frac{\partial^2 \psi}{\partial \eta^2} = -\tfrac{1}{2}(\cosh 2\xi + \cos 2\eta)\zeta, \tag{3}$$

$$\frac{\partial^2 \zeta}{\partial \xi^2} + \frac{\partial^2 \zeta}{\partial \eta^2} = \tfrac{1}{2}Re\left(\frac{\partial \psi}{\partial \eta}\frac{\partial \zeta}{\partial \xi} - \frac{\partial \psi}{\partial \xi}\frac{\partial \zeta}{\partial \eta}\right). \tag{4}$$

Their solution is required subject to the conditions

$$\psi = \partial\psi/\partial\xi = 0 \quad \text{when} \quad \xi = 0; \psi = \zeta = 0 \quad \text{when} \quad \eta = 0, \pi; \tag{5a, b}$$

$$\frac{1}{\sinh \xi}\frac{\partial \psi}{\partial \xi} \to \sin \eta, \quad \frac{1}{\cosh \xi}\frac{\partial \psi}{\partial \eta} \to \cos \eta \quad \text{as} \quad \xi \to \infty. \tag{6}$$

In practice, the computational domain of the solution is the region $0 \leqslant \xi \leqslant \xi_m$, $0 \leqslant \eta \leqslant \pi$, where ξ_m is some large enough value of ξ at which some approximate form of the conditions (6) may be assumed. This region is divided into elements by grid lines parallel to the ξ and η coordinate axes with equal spacing h in both coordinates. The equations (3) and (4) are approximated at each grid point by second-order accurate finite-difference formulae. If, in standard notation, we denote quantities at the grid points (ξ_0, η_0), (ξ_0+h, η_0), (ξ_0, η_0+h), (ξ_0-h, η_0), (ξ_0, η_0-h) by means of subscripts 0, 1, 2, 3, 4 respectively, the usual h^2-accurate approximation to (3) at (ξ_0, η_0) is

$$\psi_1+\psi_2+\psi_3+\psi_4-4\psi_0+\tfrac{1}{2}h^2(\cosh 2\xi_0+\cos 2\eta_0)\,\zeta_0 = 0, \tag{7}$$

while if we use the notation $f = \frac{1}{2}Re\,\partial\psi/\partial\eta$, $g = -\frac{1}{2}Re\,\partial\psi/\partial\xi$, we can write a generalized second-order accurate approximation to (4) at (ξ_0, η_0) as

$$\begin{aligned}(1-\tfrac{1}{2}hf_0+\alpha h^2 f_0^2)\,\zeta_1+(1-\tfrac{1}{2}hg_0+\alpha h^2 g_0^2)\,\zeta_2+(1+\tfrac{1}{2}hf_0+\alpha h^2 f_0^2)\,\zeta_3 \\ +(1+\tfrac{1}{2}hg_0+\alpha h^2 g_0^2)\,\zeta_4-(4+2\alpha h^2[f_0^2+g_0^2])\,\zeta_0 = 0,\end{aligned} \tag{8}$$

where α is a parameter to be defined.

If $\alpha = 0$, the approximation (8) is the usual central-difference representation of (4). However, the value $\alpha = \frac{1}{8}$ was suggested by Dennis & Hudson (1978) by means of an expansion procedure of an exponential scheme first given by Dennis (1960) and there is also justification for taking $\alpha = \frac{1}{12}$, since then all terms present in (8) appear as part of the h^4-accurate approximations of Dennis & Hudson (1989). All such cases of (8) are second-order accurate but the point about using non-zero values of α is that the associated matrix is diagonally dominant for all values of $\alpha \geqslant \frac{1}{16}$ and it is then known that the successive over-relaxation iterative method of solution is convergent over a well-defined range of the relaxation parameter. Iterative methods of solution were employed for solving the coupled sets of equations (7) and (8) over the given finite rectangular domain with $\alpha = \frac{1}{12}$ in (8). There is no need to describe the detail, since in principle it is similar to that used by Ingham *et al.* (1990) who used the analogue (8) with $\alpha = \frac{1}{8}$.

It may, however, be useful to give some detail of the satisfaction of the boundary conditions (5) and (6). From (6) it follows that $\zeta \to 0$ as $\xi \to \infty$ but the decay is slow in the far wake region, so as $\xi \to \infty$ we use a method of approximation to ζ originally introduced by Dennis, Hudson & Smith (1968) and used by Dennis & Chang (1970) in obtaining solutions of the vorticity equation for flow past a circular cylinder. If we linearize (4) following the manner of Oseen, using the stream function of the external stream satisfying (6), we obtain an equation which yields a solution such that $\zeta \to 0$ as $\xi \to \infty$ and from its asymptotic properties for large ξ we deduce the condition

$$\zeta(\xi+h, \eta) \sim \{\exp[z\{\cos\eta-1)-\tfrac{1}{2}h]\}\,\zeta(\xi, \eta\}, \tag{9}$$

where $z = \frac{1}{8}Re\exp(\xi)$. Equation (9) may be used as a boundary condition for (8) at some large enough value $\xi = \xi_m$ and it possesses the characteristic that, eventually, as $\xi \to \infty$, the vorticity is significant only in a region for which $z\eta^2 = O(1)$, i.e. $\eta = O(z^{-\frac{1}{2}})$ which is the correct asymptotic behaviour according to the solution of Imai (1951).

For the boundary condition for ψ at $\xi = \xi_m$, we take a perturbation Ψ from the potential flow by substituting

$$\psi = \cosh\xi\sin\eta+\Psi \tag{10}$$

in (3) and then considering the nature of the solution as $\xi \to \infty$. Since $\eta = O(z^{-\frac{1}{2}})$ as $\xi \to \infty$, the solution is of a boundary-layer nature in the η-coordinate with a boundary-layer thickness proportional to $z^{-\frac{1}{2}}$. Thus when $\xi \geqslant \xi_m$, where ξ_m is large enough, the term $\partial^2 \Psi/\partial \xi^2$ in (3), after transformation using (10), may be neglected in comparison with the term in $\partial^2 \Psi/\partial \eta^2$. In other words, as $\xi \to \infty$, (3) can be approximated by the equation and conditions

$$\frac{\partial^2 \Psi}{\partial \eta^2} = -\tfrac{1}{2}(\cosh 2\xi + \cos 2\eta)\zeta, \quad \Psi(\xi, 0) = \Psi(\xi, \pi) = 0. \tag{11a, b}$$

Once an approximation to ζ is known, therefore, at a given station $\xi = \xi_m$, a corresponding approximation to Ψ may be found by integration of (11*a*) along $\xi = \xi_m$ subject to (11*b*). Moreover, when η is large enough and ζ is asymptotically zero, the profile for Ψ is linear with η, exactly consistent with the form of solution found by Imai (1951) and used by Kawaguti (1953) in calculating flow past a circular cylinder. The solution of (11*a*) is found by two successive numerical integrations. The first integration gives

$$\left(\frac{\partial \psi}{\partial \eta}\right)_{\xi=\xi_m} = \frac{1}{\pi}\int_0^\pi F(\xi_m, \eta)\,\mathrm{d}\eta - F(\xi_m, \eta), \tag{12}$$

where

$$F(\xi_m, \theta) = \frac{1}{2}\int_0^\eta (\cosh 2\xi_m + \cos 2\theta)\,\zeta(\xi_m, \theta)\,\mathrm{d}\theta.$$

Then $\Psi(\xi_m, \eta)$ is found by a further integration of (12) subject to $\Psi(\xi_m, 0) = 0$. Thus both of (11*a*, *b*) are satisfied and then $\psi(\xi_m, \eta)$ is calculated from (10).

The conditions (5) provide complete conditions for ψ and ζ on $\eta = 0, \pi$ and for ψ on $\xi = 0$. Thus it remains only to provide a condition for ζ on $\xi = 0$ and to do this we use the condition $\partial \psi/\partial \xi = 0$ in conjunction with the finite-difference equation (7) and equation (3) to yield, following the method of Woods (1954),

$$\zeta_0 = -\frac{6\psi_1}{h^2(1+\cos 2\eta_0)} - \tfrac{1}{2}\zeta_1 \quad \text{on} \quad \xi = 0, \tag{13}$$

which is h^2-accurate. When $\eta_0 = \frac{1}{2}\pi$, (13) does not give a determination of ζ_0. The vorticity is in fact infinite at this point $\xi = 0$, $\eta = \frac{1}{2}\pi$ and this is one of the basic difficulties of the problem when the present formulation is used. We can avoid the difficulty by approximating (4) in a slightly different way at the grid point $\xi = h$, $\eta = \frac{1}{2}\pi$ following Dennis & Smith (1980). Thus, instead of approximating (4) along lines of constant ξ and η at this point, which would involve a knowledge of ζ at $(0, \frac{1}{2}\pi)$, we rotate the axes through an angle $\frac{1}{4}\pi$ which leaves (4) unaltered and then approximate the ζ derivatives in terms of $\zeta(h, \frac{1}{2}\pi)$, $\zeta(0, \frac{1}{2}\pi + h)$, $\zeta(0, \frac{1}{2}\pi - h)$, $\zeta(2h, \frac{1}{2}\pi + h)$ and $\zeta(2h, \frac{1}{2}\pi - h)$. All the points concerned are points of the grid structure but the introduction of $\zeta(0, \frac{1}{2}\pi)$ is avoided.

3. Calculated results

Calculations were carried out over the range of Reynolds numbers $Re = 0.5$ to 100 using the Gauss–Seidel iterative procedure of solution. After one complete iteration through the difference equations (7), the surface vorticity on the plate was calculated

Re	h	ξ_m	L/D	C_{D^*}
30	$\frac{1}{42}\pi$	π	3.91	1.82
30	$\frac{1}{56}\pi$	π	3.89	1.82
30	$\frac{1}{56}\pi$	$\frac{6}{5}\pi$	3.89	1.83
30	$\frac{1}{70}\pi$	π	3.84	1.82
50	$\frac{1}{60}\pi$	$\frac{7}{6}\pi$	7.12	1.55
50	$\frac{1}{60}\pi$	$\frac{4}{3}\pi$	7.13	1.55
50	$\frac{1}{80}\pi$	$\frac{47}{40}\pi$	7.03	1.57
70	$\frac{1}{80}\pi$	$\frac{101}{80}\pi$	10.84	1.41
70	$\frac{1}{80}\pi$	$\frac{9}{2}\pi$	10.87	1.41
70	$\frac{1}{100}\pi$	$\frac{13}{10}\pi$	10.50	1.42

TABLE 1. Comparisons of eddy length L and drag coefficient C_{D^*} for various h and ξ_m

from (13) and this was followed by a complete iteration through (8) in which the condition (9) was incorporated at $\xi = \xi_m$. A new boundary condition for ψ at $\xi = \xi_m$ was then calculated following the procedure outlined in the previous section. This sequence was repeated until convergence, which was decided by the criterion

$$\Sigma |\zeta^{(k+1)}(\xi, \eta) - \zeta^{(k)}(\xi, \eta)| < 0.001, \tag{14}$$

where the sum extends over all grid points and $k, k+1$ denote successive iterates. This is a more than adequate criterion in view of the fact that the surface vorticity becomes large in the neighbourhood of the singularity in ζ. It was generally necessary to use an under-relaxation factor in the calculation of the surface vorticity. The value of $\alpha = \frac{1}{12}$ was used in the difference equations (8) and this was checked using the value $\alpha = 0$ (central differences) in several cases for small enough Re, where the iterative procedures converged rapidly enough. The point here is that the iteration matrix associated with (8) when $\alpha = 0$ will lose diagonal dominance if a numerical value of hf_0 or hg_0 exceeds 2. In view of the conditions (6), this will certainly happen for a fixed Re and h when ξ becomes large and to avoid it, a balance must be chosen between Re, h and ξ_m if $\alpha = 0$ is to be used. Comparisons were carried out in the cases $\alpha = 0$, $\alpha = \frac{1}{12}$ only for $Re = 1$ and 5. The overall effect on the main computed properties of the flow of this variation of α was negligible.

The effect on the flow properties of the positioning of the outer boundary $\xi = \xi_m$ is small, owing to the employment of the asymptotic conditions noted in §2. The property most influenced by change of ξ_m is the length of the recirculating region. This can be measured quite accurately from the numerical solutions by determining the point at which the velocity component in the $x-$direction changes sign on the axis $y = 0$ at the rear of the plate, i.e. when $\eta = 0$. Thus, $\partial\psi/\partial\eta$ was calculated at grid points on $\eta = 0$ using numerical differentiation formulae of both h^2 and h^4 accuracy, which were found to agree to high precision over the whole range of Re considered. From the h^4-accurate results, the position of the zero of $\partial\psi/\partial\eta$ was estimated from Bessel's interpolation formula (Hartree, 1958, p. 68) applied to tabulated values of $\partial\psi/\partial\eta$ at the four grid points in the immediate neighbourhood of the zero, i.e. at two grid points either side of it. An illustration of the accuracy of this process will be given shortly.

In view of the comparison with experimental results to be made later, we have investigated in detail the effect of change of both ξ_m and grid size on the length of the recirculating region over the experimental range $5 \leqslant Re \leqslant 20$. The following results were obtained at $Re = 10$, but similar tests were made at $Re = 5$ and 20, with

similar results. Two grid sizes were considered, $h = \frac{1}{40}\pi$ and $\frac{1}{60}\pi$. When $h = \frac{1}{40}\pi$, the two values $\xi_m = \pi$ and $\frac{5}{4}\pi$ were considered and when $h = \frac{1}{60}$, the three values $\xi_m = \pi$, $\frac{7}{6}\pi$, $\frac{8}{6}\pi$ were used. For the grid size $h = \frac{1}{40}\pi$ the value of L/D was found to be 1.15 for both $\xi_m = \pi$ and $\frac{5}{4}\pi$ and for $h = \frac{1}{60}\pi$, L/D was found to be 1.16 for all three cases of ξ_m; it should be remembered that these three cases correspond to $x/l = 11.5$, 19.5 and 33.0, respectively, i.e. approximately 6, 10 and 16 times the breadth of the plate. The given calculated values were based on h^4-accurate values of $\partial\psi/\partial\eta$ at $\eta = 0$, but the h^2-accurate values gave practically the same results, e.g. for $h = \frac{1}{60}\pi$, $\xi_m = \pi$, the value $L/D = 1.15$ was obtained.

In order to examine the effect on the results of variation of grid we have selected two properties, one local and one global, for comparison. The local property is again the dimensionless length L/D of the separated region behind the plate and the global property is the total drag coefficient C_{D^*} corresponding to the force D^* on the plate exerted by the fluid. If we define a drag coefficient by $C_{D^*} = D^*/U^2 l$ it may be shown by consideration of the momentum balance of the fluid between the contour C_0 of the flat plate and any surrounding contour C_1 that, for any $\xi > 0$,

$$C_{D^*} = \int_0^\pi \left[\frac{2}{\cosh 2\xi + \cos 2\eta} \left\{ \left[\left(\frac{\partial\psi}{\partial\xi}\right)^2 - \left(\frac{\partial\psi}{\partial\eta}\right)^2 \right] \cosh\xi \cos\eta - 2\frac{\partial\psi}{\partial\xi}\frac{\partial\psi}{\partial\eta} \sinh\xi \sin\eta \right\} \right.$$
$$\left. + 2\left(\frac{2}{Re}\frac{\partial\zeta}{\partial\xi} - \zeta\frac{\partial\psi}{\partial\eta}\right) \cosh\zeta \sin\eta - \frac{4}{Re}\zeta \sinh\xi \sin\eta \right] \mathrm{d}\eta. \quad (15)$$

The application of (15) over various contours as ξ increases gives some indication of the accuracy of the calculations. It was found in all the cases presented that the estimate of C_{D^*} remained remarkably constant over much of the computational domain and became inaccurate only for values of ξ close to $\xi = \xi_m$.

In table 1 we give the results of some typical comparisons of the two representative properties for various Reynolds numbers and grid sizes. In general, it was found in the whole of the computations that the effect on the results of increasing ξ_m was negligible provided ξ_m was large enough and the grid size small enough. This is seen, for example, at $Re = 50$ in table 1, where an increase in ξ_m from $\frac{7}{6}\pi$ to $\frac{4}{3}\pi$ when $h = \frac{1}{60}\pi$ increases L/D by a very small amount and again at $Re = 70$ in the case of $h = \frac{1}{80}\pi$, where L/D increases only from 10.84 to 10.87 as ξ_m is increased from $\frac{101}{80}\pi$ to $\frac{3}{2}\pi$. The effect of decrease of grid size is more important, e.g. for both $Re = 50$ and 70. Thus the values $\xi_m = \frac{7}{6}\pi$, $\frac{47}{40}\pi$ are roughly the same for two of the solutions at the same value $Re = 50$ and there is about a 1% difference in L/D. There is a greater change with grid size of L/D for the two solutions at the approximately same values of $\xi_m = \frac{101}{80}\pi$ and $\frac{13}{10}\pi$ at $Re = 70$. However, the change is only about 3% and the more accurate of the two values probably differs from the correct value by less than this amount. Finally, a test of the accuracy of the equation (13) employed to calculate the surface vorticity on the plate has been made by using an alternative method in which the vorticity at $\xi = 0$ is determined from integrals involving the vorticity throughout the field of flow derived from one of Green's identities. This method has been described by Dennis & Chang (1969) and more generally by Dennis & Quartapelle (1989), where a test of this method is given for the case $Re = 70$ of the present problem. The surface vorticity is found to differ little from the calculation using (13), although the difference is rather more near the singularity at $\eta = \frac{1}{2}\pi$. Nevertheless, the effect on the overall properties is insignificant.

In table 2, the results obtained from the present computed solutions corresponding

Re	h	ξ_m	L/D	a/D	b/D	C_{D^*}
0.5	$\frac{1}{42}\pi$	π	0.12	0.07	0.44	15.08
1	$\frac{1}{42}\pi$	π	0.21	0.10	0.51	9.66
5	$\frac{1}{60}\pi$	$\frac{4}{5}\pi$	0.65	0.27	0.59	3.75
10	$\frac{1}{60}\pi$	$\frac{4}{5}\pi$	1.16	0.46	0.62	2.75
20	$\frac{1}{60}\pi$	$\frac{4}{5}\pi$	2.43	0.68	0.78	2.09
30	$\frac{1}{70}\pi$	$\frac{6}{5}\pi$	3.89	1.00	0.87	1.82
40	$\frac{1}{60}\pi$	$\frac{6}{5}\pi$	5.48	1.45	0.99	1.68
50	$\frac{1}{80}\pi$	$\frac{6}{5}\pi$	7.03	1.97	1.15	1.57
70	$\frac{1}{100}\pi$	$\frac{13}{10}\pi$	10.50	3.53	1.36	1.42
100	$\frac{1}{130}\pi$	$\frac{3}{2}\pi$	15.3	6.54	1.64	1.34

TABLE 2. Calculated properties of the solution

Re	h	$L/(DRe)$	$a/(DRe)$	$b/(DRe^{\frac{1}{2}})$	$y_w/(DRe^{\frac{1}{2}})$
1	$\frac{1}{42}\pi$	0.21	0.10	0.51	0.97
5	$\frac{1}{42}\pi$	0.13	0.052	0.26	0.44
10	$\frac{1}{42}\pi$	0.12	0.046	0.20	0.33
20	$\frac{1}{42}\pi$	0.12	0.034	0.17	0.29
30	$\frac{1}{70}\pi$	0.13	0.033	0.17	0.28
40	$\frac{1}{60}\pi$	0.14	0.036	0.16	0.28
50	$\frac{1}{80}\pi$	0.14	0.039	0.16	0.28
70	$\frac{1}{100}\pi$	0.15	0.048	0.16	0.28
100	$\frac{1}{130}\pi$	0.15	0.065	0.16	0.28

TABLE 3. Properties of the solutions scaled with respect to Reynolds number

to the smallest grid sizes are presented for several properties, including the length of the separated region L and the coordinates (a, b) of the vortex centre. The results show good overall agreement with the corresponding results of Hudson & Dennis (1985, p. 377) over the range $Re = 0.5$ to 20. The streamlines and equivorticity lines for $0.5 \leqslant Re \leqslant 20$ compare well with those of Hudson & Dennis (1985). Some typical streamlines and equivorticity lines are given in figures 2 and 3. In table 3, we give values of various quantities scaled with respect to either Re or $Re^{\frac{1}{2}}$ in accordance with the expected theoretical behaviour of Smith (1979, 1985) and Peregrine (1985) noted in the present introduction. The quantity y_w is the half-breadth of the separated region. There is certainly a tendency of $L/(DRe)$ and $y_w/(DRe^{\frac{1}{2}})$ to become constant at the upper range of Re consistently with the numerical work of Fornberg (1980, 1985) for a circular cylinder and the behaviour of the coordinates of the vortex centre seems to be consistent with the trend of L and y_w.

It is clear from both table 3 and figure 2 that the evolution with Re of the calculated wake-length is much greater in the present problem than in the case of the infinite cascade of plates considered by Ingham *et al.* (1990). They have carried out calculations corresponding to the single blockage ratio $\beta = 2.0$, where β is the ratio of the distance between successive gaps in the cascade to the plate breadth. Calculations as $\beta \to \infty$ would presumably be needed to relate their work to the present calculations and experiments. Finally, in the case of the present problem, figures 4 and 5 give calculated velocity distributions on the axis of symmetry before and after the plate which were not given by Hudson & Dennis (1985). The distributions in figure 5, together with various other properties of the motion for $Re \leqslant 20$ which have

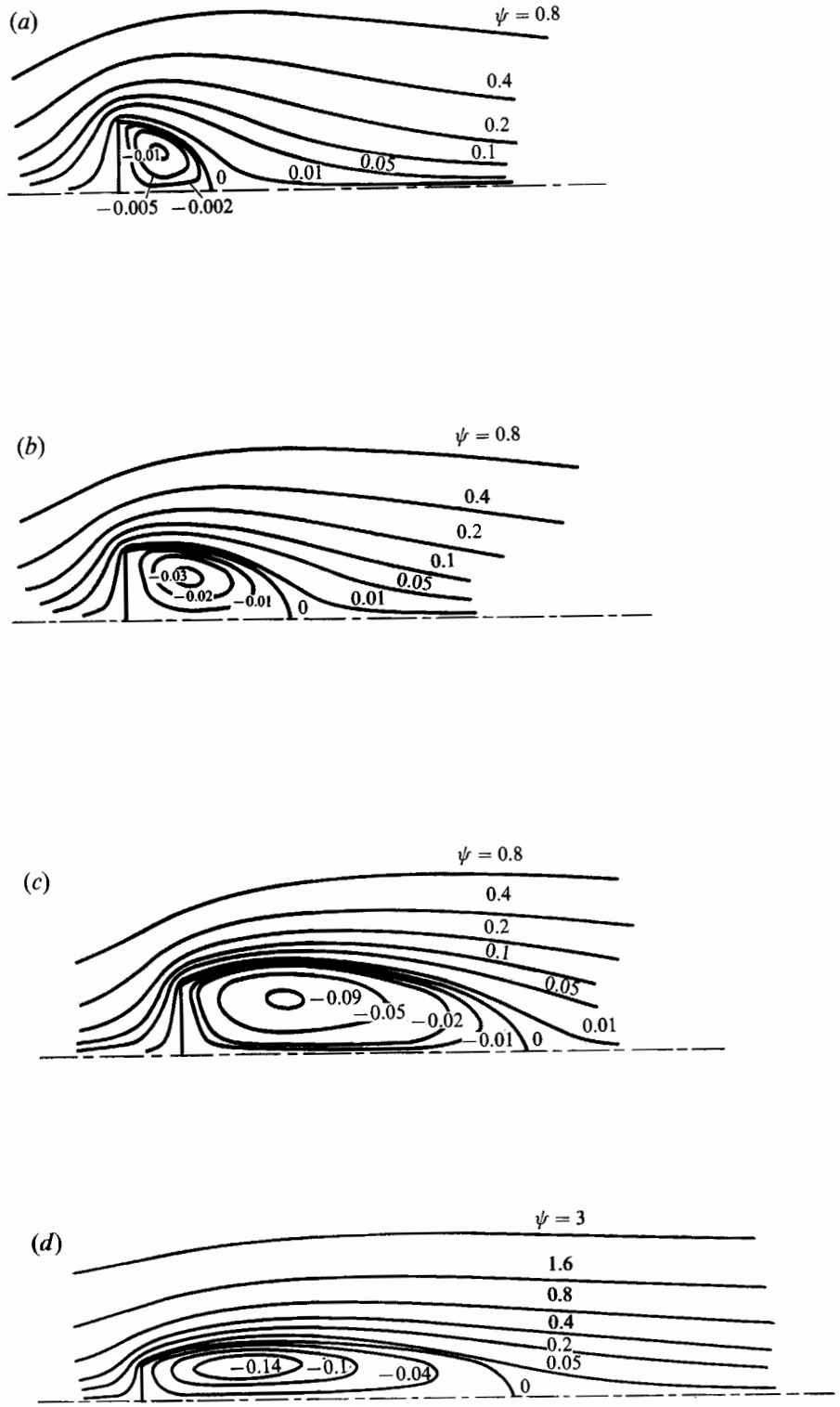

FIGURE 2 (*a–d*). For caption see facing page.

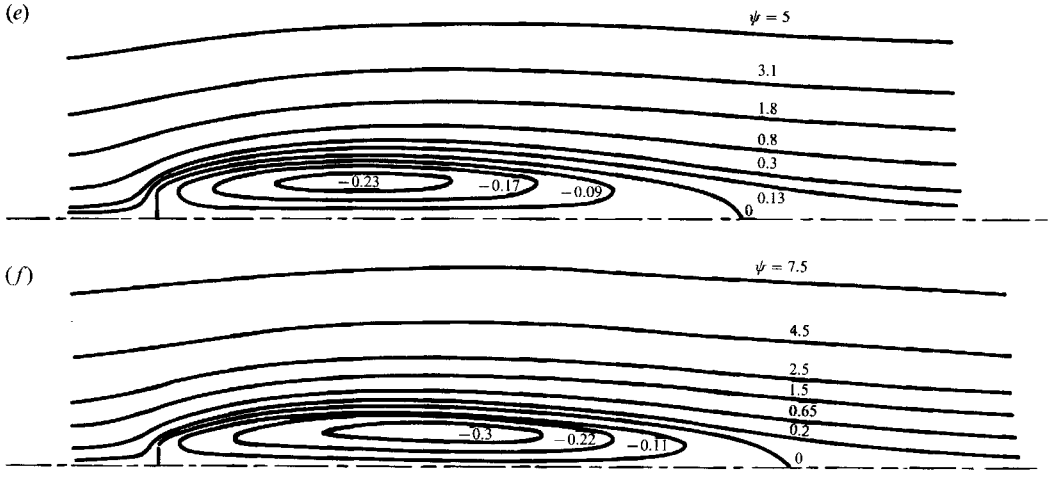

FIGURE 2. Streamlines for steady flow normal to a flat plate in an unbounded fluid. Values shown are for the dimensionless stream function ψ. (*a*) $Re = 5$; (*b*) $Re = 10$; (*c*) $Re = 20$; (*d*) $Re = 40$; (*e*) $Re = 70$; (*f*) $Re = 100$.

been presented in the present section, will be related to corresponding experimental results later.

4. The experimental technique and parameters

The experimental technique is based on the same general principle as that used previously for studying similar flows at the Laboratoire de Mécanique des Fluides of the Université de Poitiers and is described, for example, in Coutanceau & Bouard (1977*a*, *b*), Maalouf & Bouard (1987), Ohmi *et al.* (1990). Thus, using solid tracers lit by a thin sheet of light coming from a powerful arc projector, we have visualized at different stages of its development a cross-section of the flow induced by a flat plate which is impulsively subjected, from rest, to a constant translational velocity U perpendicular to itself. The photographs are taken sequentially with a suitable time of exposure in order to obtain quasi-instantaneous velocity fields. The camera is controlled automatically by a micro-computer as it accompanies the plate in its motion simultaneously with a sheet of light which is created by a rotating mirror. Thus, in this frame, the plate appears to be fixed and placed normally to the uniform stream U, as shown in figure 1; details of the experimental conditions are given in table 4. By means of a semi-automatic analysis of the pictures using a geometrical table connected to a micro-computer, we have been able to determine the main characteristics of the recirculating zone which is formed at the rear of the plate, such as the length L and the coordinates (a, b) of the vortex centres (see figure 1), together with the velocity distribution along the rear axis of the flow. It is, in fact, the accurate determination of the point of reversal of this axial velocity component which allows us to determine the length L accurately. The error of this determination is certainly less than 5%, often considerably so. The evolution of these properties of the flow as a function of the normalized time $t^*(= Ut/D)$, the Reynolds number $Re = UD/\nu$ and the blockage ratio $\lambda = D/A$ have been studied for the values given in table 5.

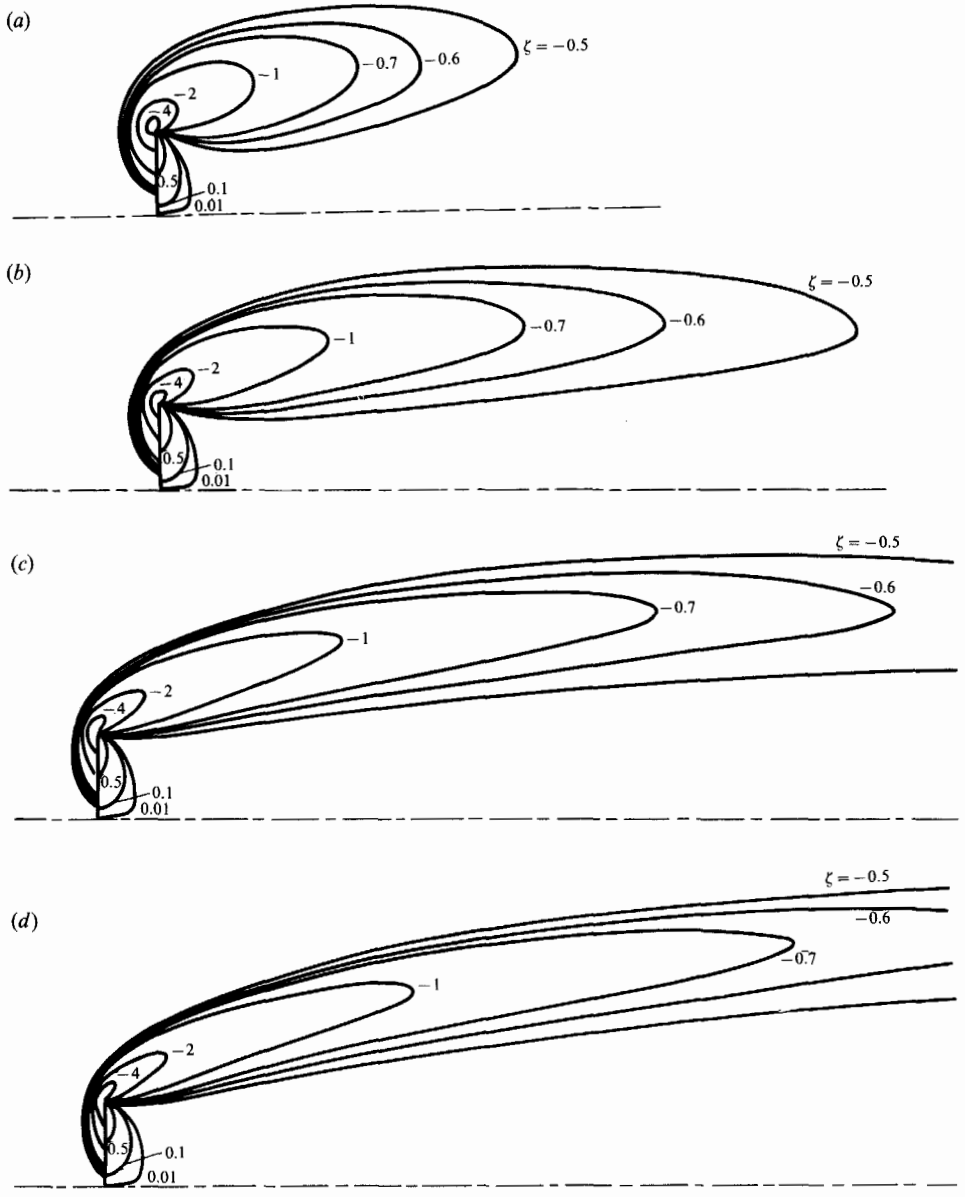

FIGURE 3. Equivorticity lines for steady flow normal to a flat plate in an unbounded fluid. Values shown are for the dimensionless vorticity ζ. (*a*) $Re = 20$; (*b*) $Re = 40$; (*c*) $Re = 70$; (*d*) $Re = 100$.

5. Description of the unsteady flow

In the present section we shall study the development of the unsteady flow with time until a steady-state regime is established. Results of the flow visualizations will be presented and also the details of some results for the evolution with time of the velocity distributions on the axis of symmetry downstream of the plate. The main characteristics of all of the results are in principle the same. A separated region of flow appears to the rear of the plate consisting of two counter-rotating vortices, each with its own centre. This separated region elongates as time proceeds until eventually its length approaches a constant value and the vortex centres assume positions

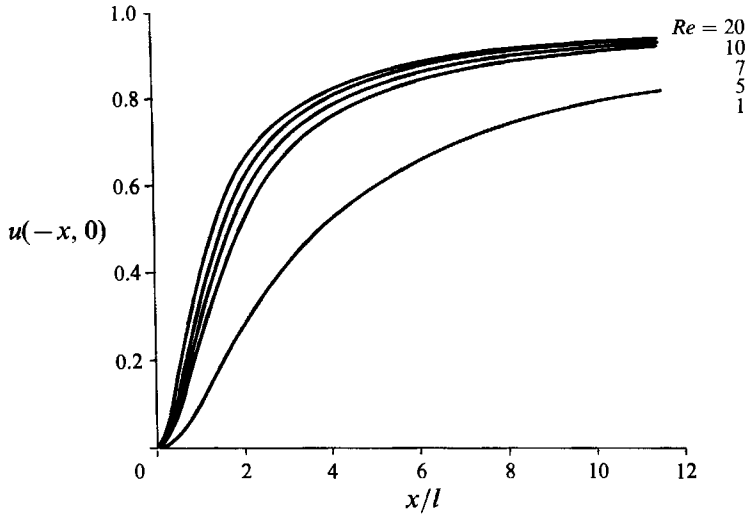

FIGURE 4. Dimensionless axial velocity distribution u on the axis of symmetry in front of the plate.

independent of time. It is these steady-state results which may be compared with the calculations.

As an example, in figure 6, we show a series of visualizations giving the time evolution of the flow for the fixed Reynolds number $Re = 20$ and the blockage ratio $\lambda = 0.2$. The experimental arrangements are such that the plate is seen end-on by the lens, which tends to cause a blurring on the photographs because the end of the plate is not in the field of vision of the camera (i.e. in the visualized plane). It may also appear from some of the photographs that the plate is not precisely perpendicular to the oncoming flow, but this is not the case. The illusion is due to the fact that the photographs are not taken at the same vertical position of the plate during its downward motion and the direction of the accompanying sheet of light is not exactly the same as the plate since it does not follow the motion of the plate precisely. This causes a shadow, which can appear inclined to the flow on the photographs. Actually, the plate is always maintained exactly at right angles to the direction of motion since the slightest asymmetry in the vortices would cause instability of the flow. The evolution with time of the velocity distribution on the axis of symmetry at the rear of the plate which corresponds to the flow development given in figure 6 is indicated in figure 7. We have already noted that the intersection of these curves with the x-axis gives the length of the recirculating zone.

The very rapid evolution of the flow in the initial stages of the motion and the very much slower later evolution from $t^* = 2.5$ is very clear from figure 7. One can see that the velocities in the wake and the length of the separated region have practically stabilized from $t^* = 4$. However, as has already been noted in previous studies of flow around a circular cylinder (Coutanceau & Bouard 1977*a*, *b*), the flow still continues to evolve slightly outside the wake. In fact, it is found that the steady-state regime is established more rapidly inside the recirculating region than outside it. We see also from figure 7 that the maximum velocity in the axial returning flow increases initially until $t^* = 1.5$ and displaces towards the rear, but then after $t^* = 1.5$ the maximum velocity decreases as it approaches the steady-state value. At $t^* = 1.5$ this maximum velocity is about 1.6 times greater than the limiting value attained at $t^* = 4$. The same phenomenon occurs for other blockage ratios.

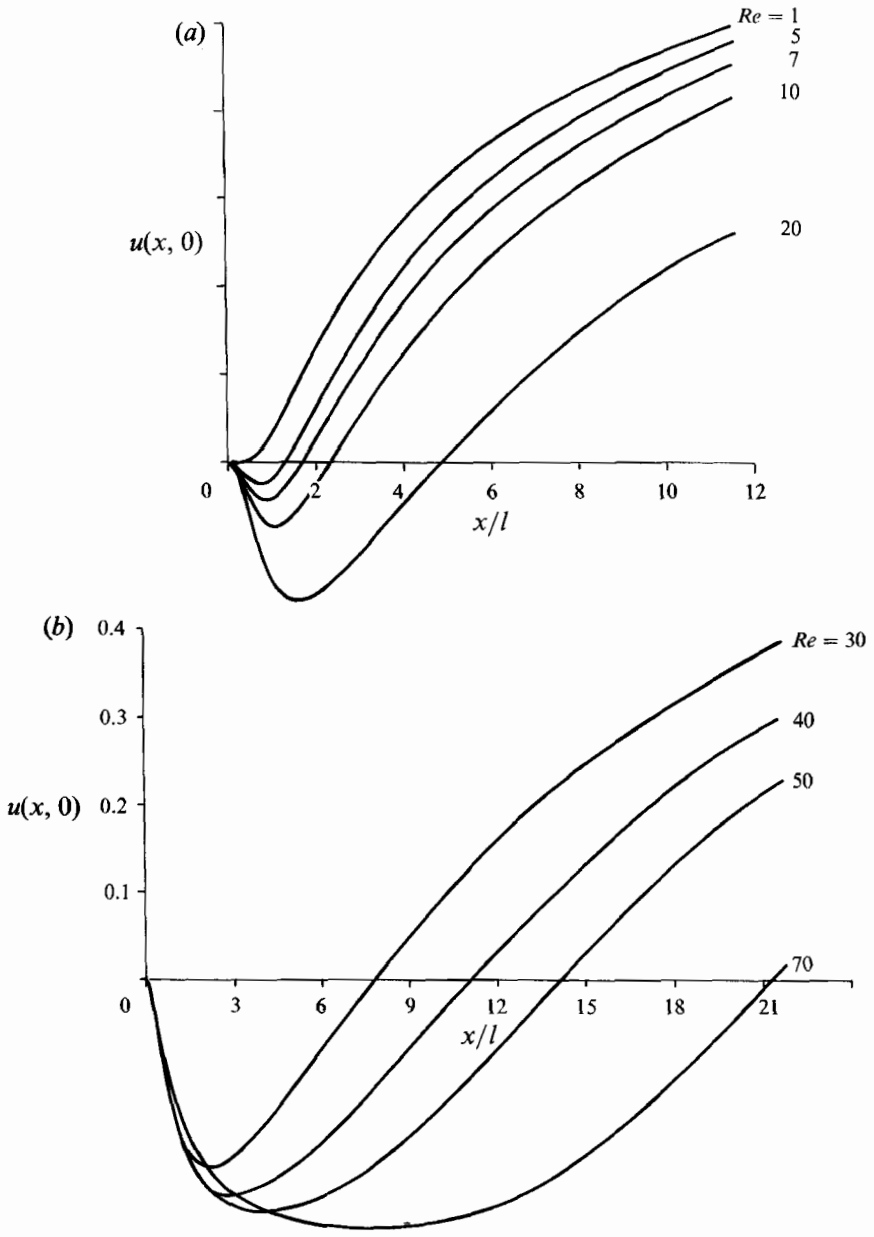

FIGURE 5. Dimensionless axial velocity distribution u on the axis of symmetry to the rear of the plate. (*a*) $1 \leqslant Re \leqslant 20$; (*b*) $30 \leqslant Re \leqslant 70$.

We next consider, in figure 8(*a*), the development with time of the recirculating region for the same Reynolds number $Re = 20$ but for different blockage ratios λ. The evolution is practically the same for all values of λ until about $t^* = 2$, at which the length of the wake is already about 1.4 times the breadth of the plate. We have included in figure 8(*a*) the results obtained from the calculations of Hudson & Dennis (1985) together with those of the present paper. They are situated very reasonably above the experimental limiting values and they indicate the very important effect of the confinement of the channel walls. Thus, for the smallest blockage ratio, i.e.

Geometrical parameters		
Flat plate	width D	= 2.8 or 5.6 or 8.4 or 11.2 cm
	length h	= 43 cm
	thickness e	= 3 mm
Tank	cross-section	56 × 46 cm²
	height	1 m
		(the useful distance of displacement of the model is only 50 cm)
Reflex camera		6 × 6
Working liquid		Oil Primol 352 ν = 220 cst for 20°
Solid tracers		Cuttings of magnesium of 4–5 μm thickness and 20–40 μm length. Density: 1.74
Range of speeds		0.5 cm/s $\leqslant U \leqslant$ 8.5 cm/s
Exposure time		0.5 s $\leqslant$ tp $\leqslant$ 8 s

TABLE 4. Details of the experimental parameters

D = 11.2 cm λ = 0.20	Re = 20 − 10 − 7 − 5	$0 \leqslant t^* \leqslant 5$ with $\Delta t^* = 0.5$
D = 8.4 cm λ = 0.15	Re = 20 − 10 − 7 − 5	$0 \leqslant t^* \leqslant 7$ with $\Delta t^* = 0.5$
D = 5.6 cm λ = 0.10	Re = 20 − 10 − 5	$0 \leqslant t^* \leqslant 9$ with $\Delta t^* = 0.5$
D = 2.8 cm λ = 0.05	Re = 10 − 5	$0 \leqslant t^* \leqslant 12$ with $\Delta t^* = 0.5$

TABLE 5. Parameter values used in the experiments

$\lambda = 0.1$, the length of the recirculating zone appears to be already about 20% smaller than it would be in an unbounded fluid and for $\lambda = 0.2$ it is 33% smaller. This is in good agreement with the results obtained previously in the case of a circular cylinder (Coutanceau & Bouard 1977*a*, *b*) where, for the same Re, a reduction of 22% and 35% was found from experiments for $\lambda = 0.07$ and 0.12 respectively compared with the corresponding wake length in an unbounded fluid obtained by extrapolation.

For $Re = 10$ the evolution with time of the wake is shown for $\lambda = 0.05$, 0.1, 0.15 and 0.2 in figure 8(*b*). For this smaller value of Re, the approach to a steady state is more rapid for all values of λ than for $Re = 20$. A particular feature for this Reynolds number is that for a given value of λ the wake length L passes through a maximum before eventually decreasing to its final steady-state value. This is clearly seen for $\lambda \geqslant 0.1$. It is also clear from this figure that the confinement of the channel does not affect the initial development of the wake length, but only starts to exert an effect somewhere after $t^* = 1$. We have noted a similar situation in figure 8(*a*) up to about $t^* = 2$ and it is found again in figure 8(*c*) ($Re = 5$) up until about $t^* = 0.5$. It seems, therefore, that the influence of the walls is not significant for approximately the same initial period of actual time t in each case. Moreover, the approach to the steady state is more rapid for the larger blockage ratios.

A study has also been made of the evolution with time of the position of the centres of the twin vortices for each of the values of Re and λ considered. The notation is indicated in figure 1. As an example, figure 9 shows the variation of the normalized distance a/D from the plate to a vortex centre with time for the case of $Re = 10$ and

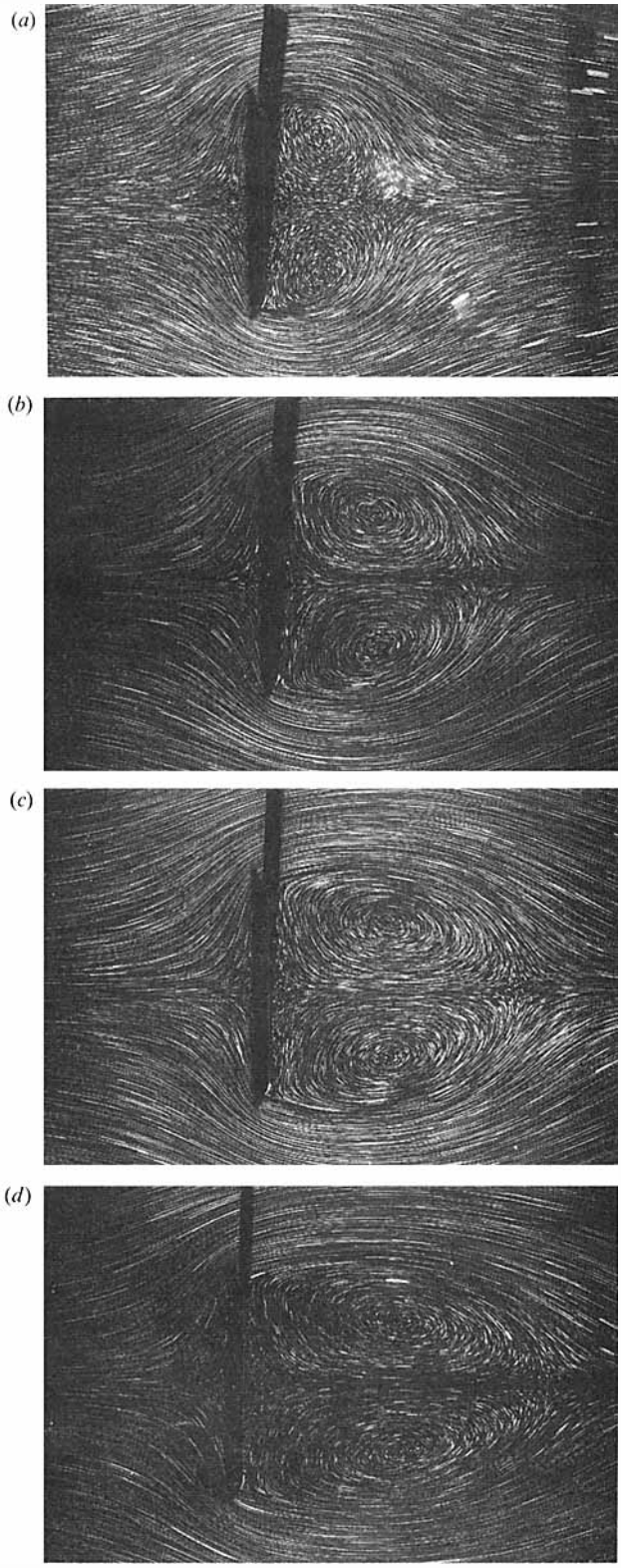

FIGURE 6(*a–d*). For caption see facing page.

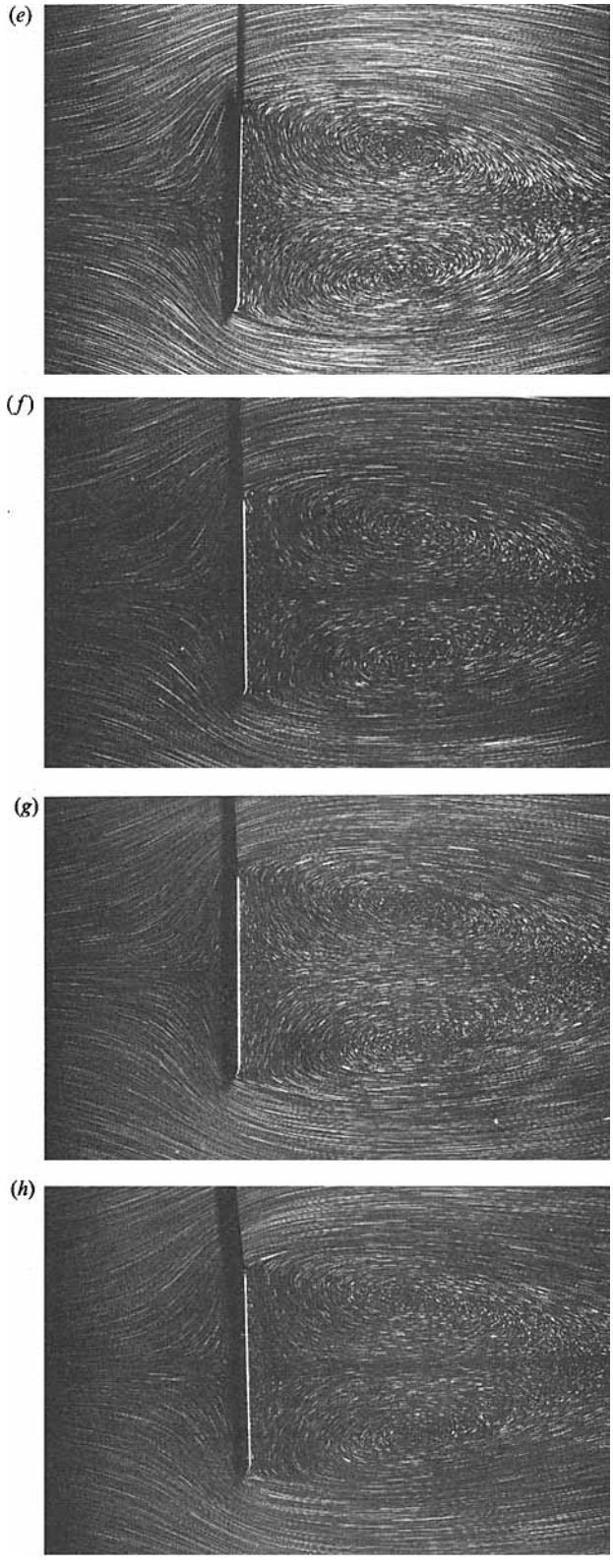

FIGURE 6. A series of flow visualizations for $Re = 20$ and blockage ratio $\lambda = 0.2$. $t^* =$ (*a*) 0.5; (*b*) 1.0; (*c*) 1.5; (*d*) 2.0; (*e*) 2.5; (*f*) 3.0; (*g*) 3.5; (*h*) 4.0.

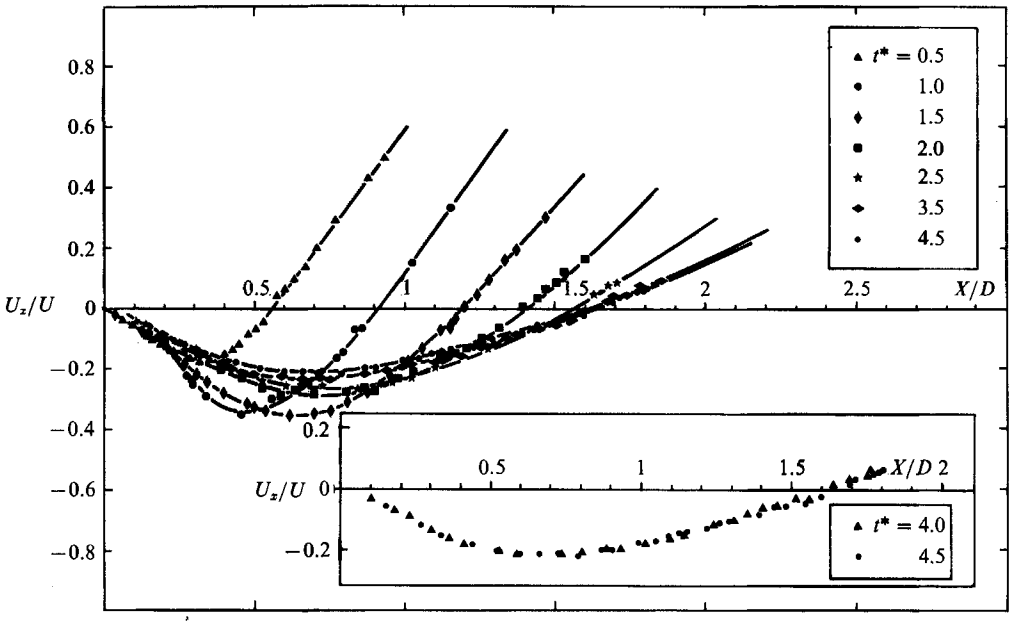

FIGURE 7. Velocity distribution on the rear flow axis for different times t^* when $Re = 20$, $\lambda = 0.20$.

various values of λ. The evolution is analogous to that of the length of the wake but with a rate of increase which is about twice as slow. The limiting steady-state values depend very little on the blockage ratio and the whole development of a/D is affected very much less by the variation of λ than the development of the length of the wake. This indicates that the vortices are deformed by the presence of the walls and the centres are displaced only very slightly towards the rear as λ decreases.

The evolution with time of the distance between the centres of the twin vortices is indicated for $Re = 10$ in figure 10, which gives curves of b/D versus t^* for various values of λ. As in the case of figure 9 for a/D, there is very little change in the curves as λ varies, although a slight increase of b/D takes place as λ decreases. In fact there is little change in the ratio b/D with either Reynolds number or λ; we shall illustrate this point later for the steady-state results when we consider the variation of the limiting values of a, b and L with both Re and λ.

An interesting comparison confirming our experimental results for L/D may be made with those of Taneda & Honji (1971) for Re about 20 and $\lambda = 0.026$ (figure 11). If we take into account the lack of initial influence of the confining walls, an excellent agreement is found. In effect, during the initial time $t^* < 4$ our curve for $Re = 20$ is exactly between theirs for $Re = 18.1$ and 24.3, while above $t^* = 4$, the overall effect of the greater confinement causes the recirculating zone to be established more rapidly with a shorter length.

6. Comparisons with steady-state calculations

We now compare the steady-state results obtained in the experiments with the calculations of Hudson & Dennis (1985) and with the new results by obtaining extrapolated estimates to $\lambda = 0$ of the effect of the blockage ratio λ. Extrapolation is obviously necessary from figure 8; however, figures 8–10 show clearly the fact that

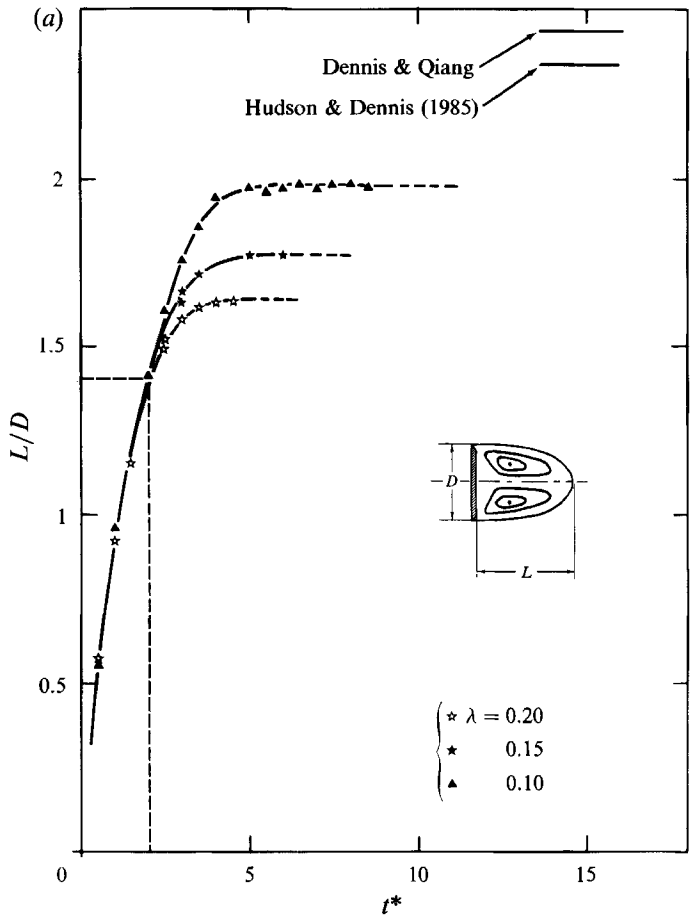

FIGURE 8(*a*). For caption see page 625.

a true steady state has been obtained in the experiments. The steady-state structure of the flow is given in figure 12. We should point out that (*a*) and (*c*) correspond to the smallest plate used, (*b*), (*d*) and (*e*) to the medium plate and (*f*) to the largest one. The dimensions of the plates are, of course, governed by the Reynolds number required and the viscosity of the fluid used. Two visualizations are given for each λ; thus, for $Re = 5$, 10 and 20, the figures show clearly the influence of both the Reynolds number and the blockage ratio. Each figure for the smallest λ compares well, where appropriate, with figure 2, bearing in mind the effect of λ. A method of extrapolation to $\lambda = 0$ of the various properties is to fit the values for the three smallest values of λ to a parabolic approximation which can then be used to continue the curves to $\lambda = 0$. Indeed, this is the only reasonable means of extrapolating these empirical results and the rate of variation with λ of the properties is not greatly different from linear, generally speaking.

In figure 13, we show the steady-state results for the wake length as a function of the blockage ratio λ. Two curves are shown for each of the Reynolds numbers, depending on whether the length L is measured from the front or the rear of the plate, i.e. the curves correspond to L/D and $(L+e)/D$, where e is the thickness of the plate. This introduces the point that the plate is of finite thickness, having the form

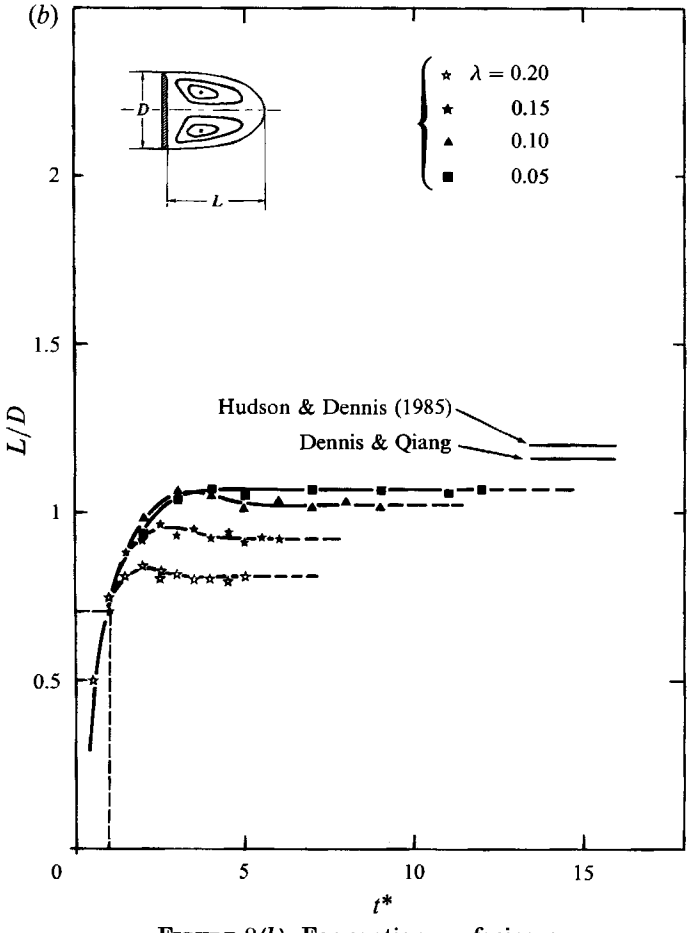

FIGURE 8(b). For caption see facing page.

indicated in figure 1, whereas the calculations are performed for an infinitesimally thin plate. Thus, it is not completely clear as to which is the appropriate comparison and, whereas this may be of relatively small importance at $Re = 20$ when the wake is longer, it could introduce more error at $Re = 5$, when it is shorter. However, the comparison is seen to be satisfactory, since for $Re = 5$ and 10 the calculated results lie between the two estimates L/D and $(L+e)/D$ and for $Re = 20$ at least one of the calculated results lies between the two.

An attempt was, in fact, made in the calculations to consider the effect of finite thickness by considering a very thin elliptic cylinder of the same ratio e/D as the plate. In each case the plate thickness in the experiments is $e = 3$ mm (so that from table 4, giving the plate breadths, we obtain $0.026 \leqslant e/D \leqslant 0.107$). Thus, detailed calculations were carried out at $Re = 10$ over this range. However, for the case of an elliptic cylinder, it was found that separation occurs on the downstream surface after the fluid has passed the ends of the major axis, so it is difficult to make precise comparisons with the flow indicated in figure 1. The thickness of the plate as well as the profile indicated in figure 1 are governed by technical considerations of construction. Thus, these finer details of the comparisons are not entirely settled but it seems appropriate to mention them in an experimental–numerical investigation of the present kind.

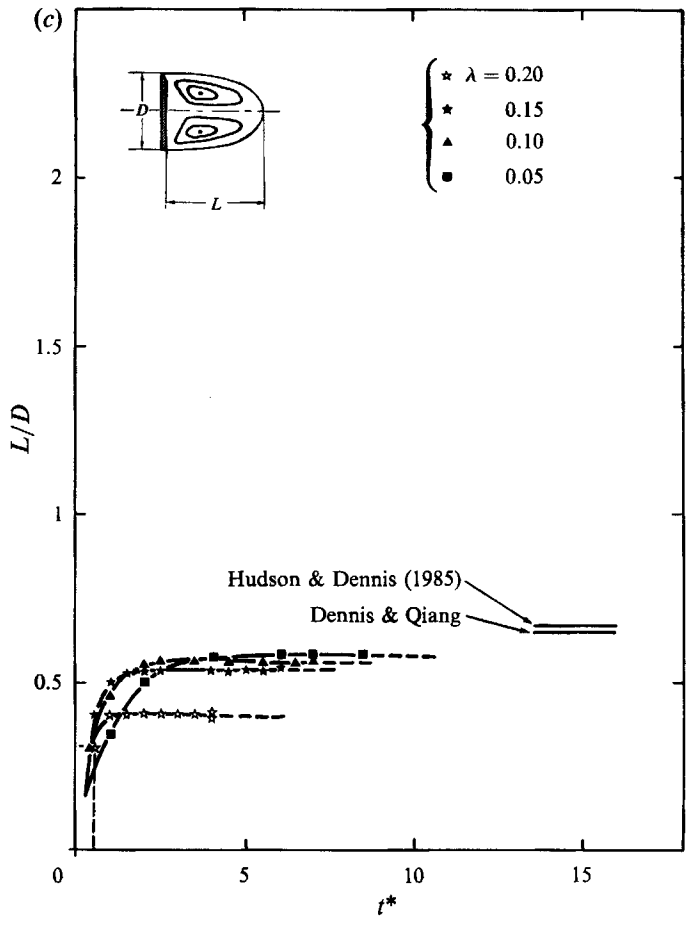

FIGURE 8. Evolution with time t^* of the flat plate closed-wake length for (*a*) $Re = 20$, (*b*) $Re = 10$, (*c*) $Re = 5$, and for different λ values.

The variation with Re of the various steady-state estimates of L/D is shown in figure 14. As we have previously noted, the results of Ingham *et al.* (1990) are considerably lower than those of the present calculations and seem to coincide with the present experimental results for blockage ratio $\lambda = 0.1$. The experimental results for the dependence on λ of the steady-state distance between the plate and the centre of each of the twin vortices is shown in figure 15. The variation is not great for any of the values of Re but the estimates are somewhat higher than those of the calculated results. The results of figure 16 for the distance between the two vortex centres also indicate very little variation with λ in the experiments.

A summary of results relating to the experimental and calculated positions of the vortex centres is given in table 6. The experimental values indicate the range of variation of a/L and b/d, where d is the maximum width of the bubble, over the range of λ considered. The calculations correspond to $\lambda = 0$. As we have already mentioned, the calculations for a/L seem to be on the low side. However, the range of variation of b/d in the experiments is small and quite consistent with the approximately constant value given by Hudson & Dennis (1985). Thus, taken in conjunction with the good measure of agreement between the calculations and the

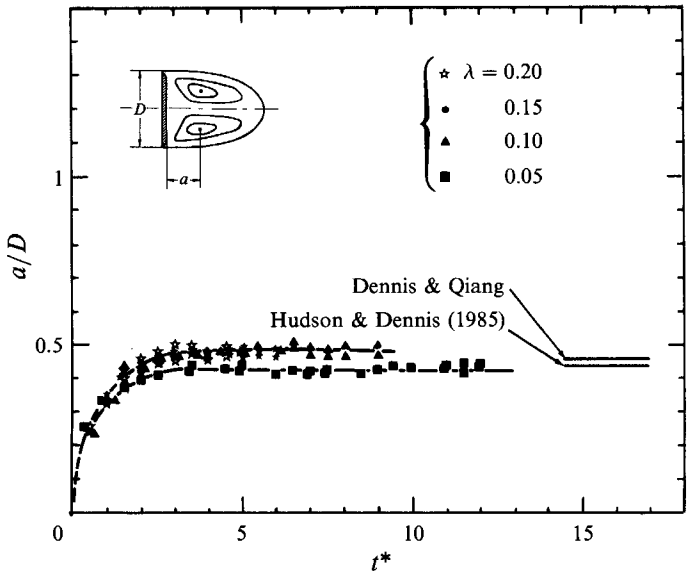

FIGURE 9. Evolution with time t^* of the distance between the flat plate and the vortex centre for $Re = 10$ and different λ values.

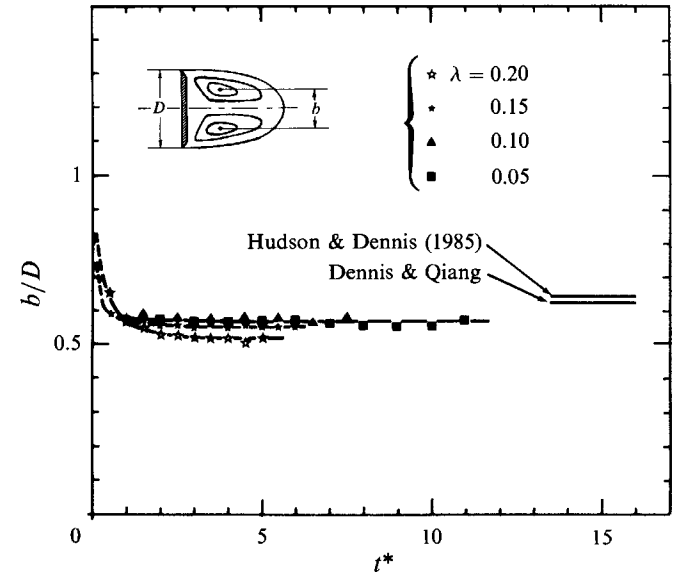

FIGURE 10. Evolution with time t^* of the distance between the two vortex centres for $Re = 10$ and different λ values.

experimental results of figures 13 and 14 for the length of wake, we may suppose that the overall agreement between theory and experiment is good.

Finally, we give some results for the velocity distribution on the axis of symmetry to the rear of the plate in figure 17. This velocity distribution depends, naturally, on the blockage ratio λ in the experimental results. However, it is found that, by normalizing the velocity with respect to the maximum velocity $Ux_{\max}$ and the x-distance by the wake length L, the curves of $Ux/Ux_{\max}$ can be sensibly compared

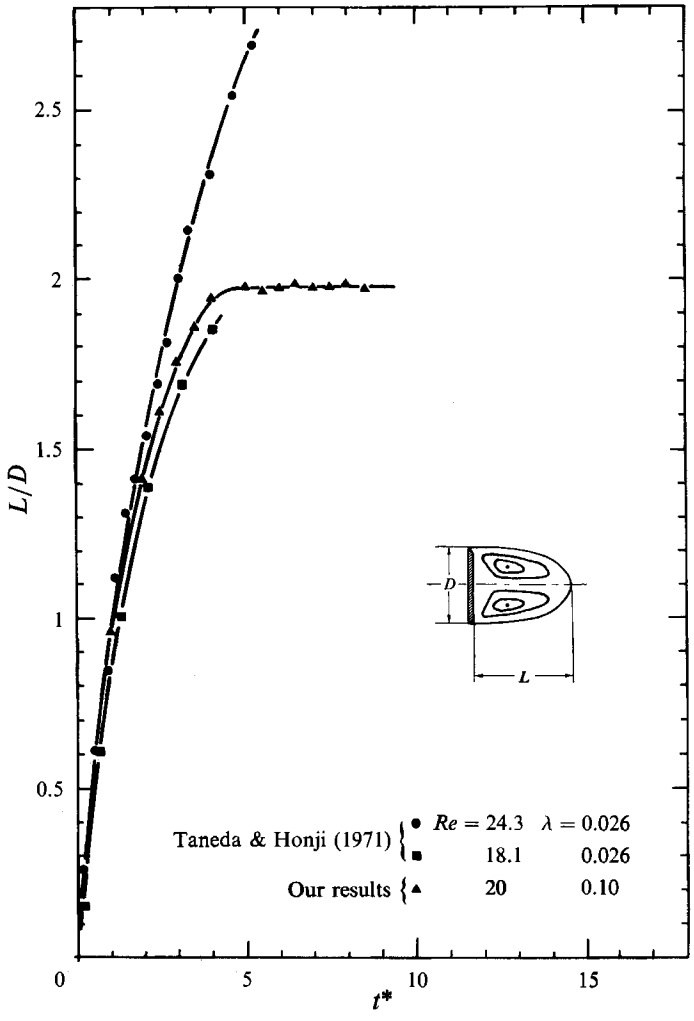

FIGURE 11. Evolution with time t^* of the flat plate closed-wake length.

with the calculations corresponding to $\lambda = 0$. Such a comparison is made for $Re = 10$ in figure 17(a), and for $Re = 20$ in figure 17(b). We may note in both figures that decrease of λ causes the experimental values of $Ux/Ux_{\max}$ to increase at stations which are closer to the plate than the location of $Ux_{\max}$ and to decrease at stations farther away from the plate than this location. In effect, the profiles of $Ux/Ux_{\max}$ are displaced towards the plate as $\lambda \to 0$. Moreover, the calculated results are completely consistent with this tendency and are located more or less where one might expect the limit $\lambda = 0$ of the experimental results to be.

Figure 17 indicates that, for each value of Re, the tendency of the location of the maximum axial velocity to move towards the plate as $\lambda \to 0$ is similar to the corresponding movement towards the plate of the vortex centre. There is also a tendency of the location of the maximum velocity for a given λ to move towards the plate as Re increases. Thus, for example, the location of each of the maximum values of the axial velocity in the experiments for different λ, which is displaced only slightly towards the plate from the location $x/L = 0.5$ at $Re = 10$ in figure 17(a), has

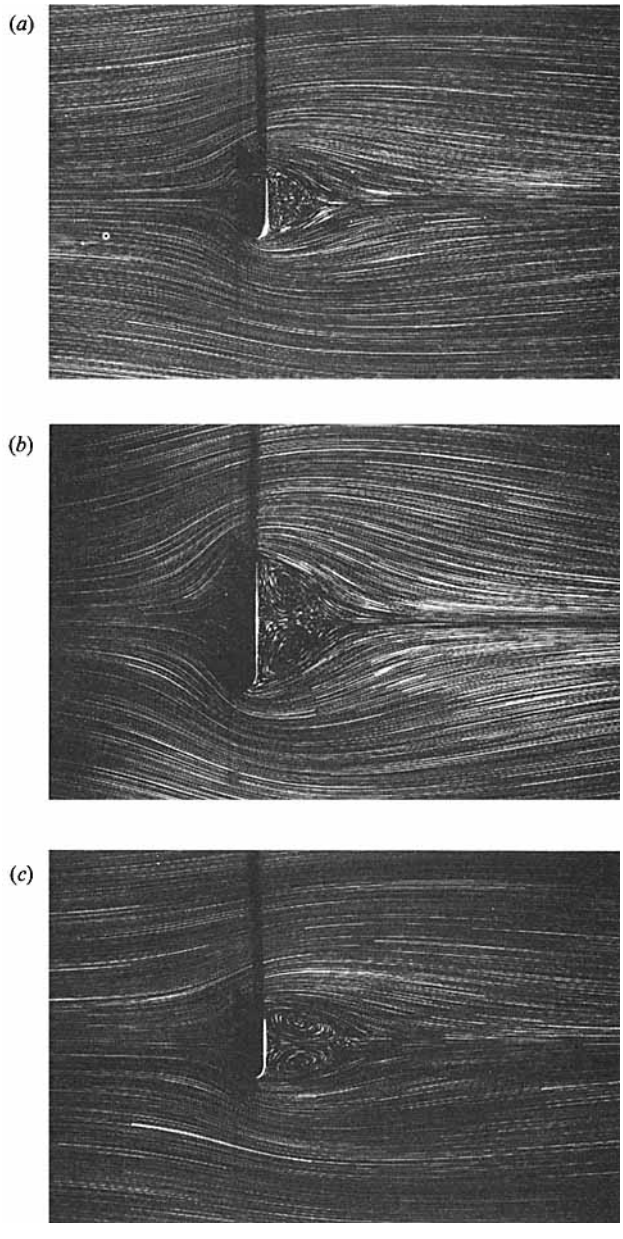

FIGURE 12(*a–c*). For caption see facing page.

moved nearer to the plate in figure 17(*b*) at $x/L = 0.4$ when $Re = 20$. This is entirely consistent with calculations and, indeed, consistent with the trend seen in figure 17. For example, the position of the maximum axial velocity for $\lambda = 0$ at $Re = 10$ in figure 17(*a*) is at $x/L = 0.44$, according to the calculations, and at $Re = 20$, in figure 17(*b*), it has moved to $x/L = 0.31$.

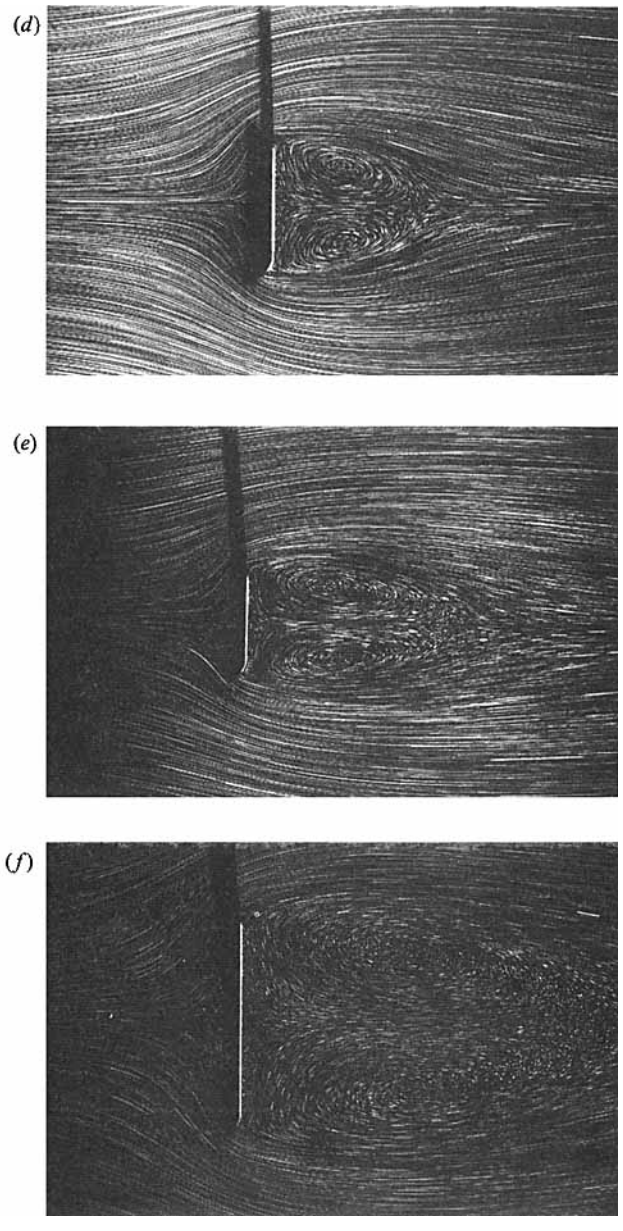

FIGURE 12. The steady-state structure of the flow. (*a*) $Re = 5$, $\lambda = 0.05$; (*b*) $Re = 5$, $\lambda = 0.10$; (*c*) $Re = 10$, $\lambda = 0.05$; (*d*) $Re = 10$, $\lambda = 0.10$; (*e*) $Re = 20$, $\lambda = 0.10$; (*f*) $Re = 20$, $\lambda = 0.20$.

7. Summary and conclusion

The experimental part of this study has allowed us to obtain results for the unsteady flow normal to a flat plate in a channel which indicate how the effect of the walls changes the configuration of the flow. No systematic study of the influence of the walls on the wake behind a flat plate seems to have been made up to now. We have measured the velocity distribution on the axis of symmetry behind the plate, determined the different parameters which characterize the nature of the wake

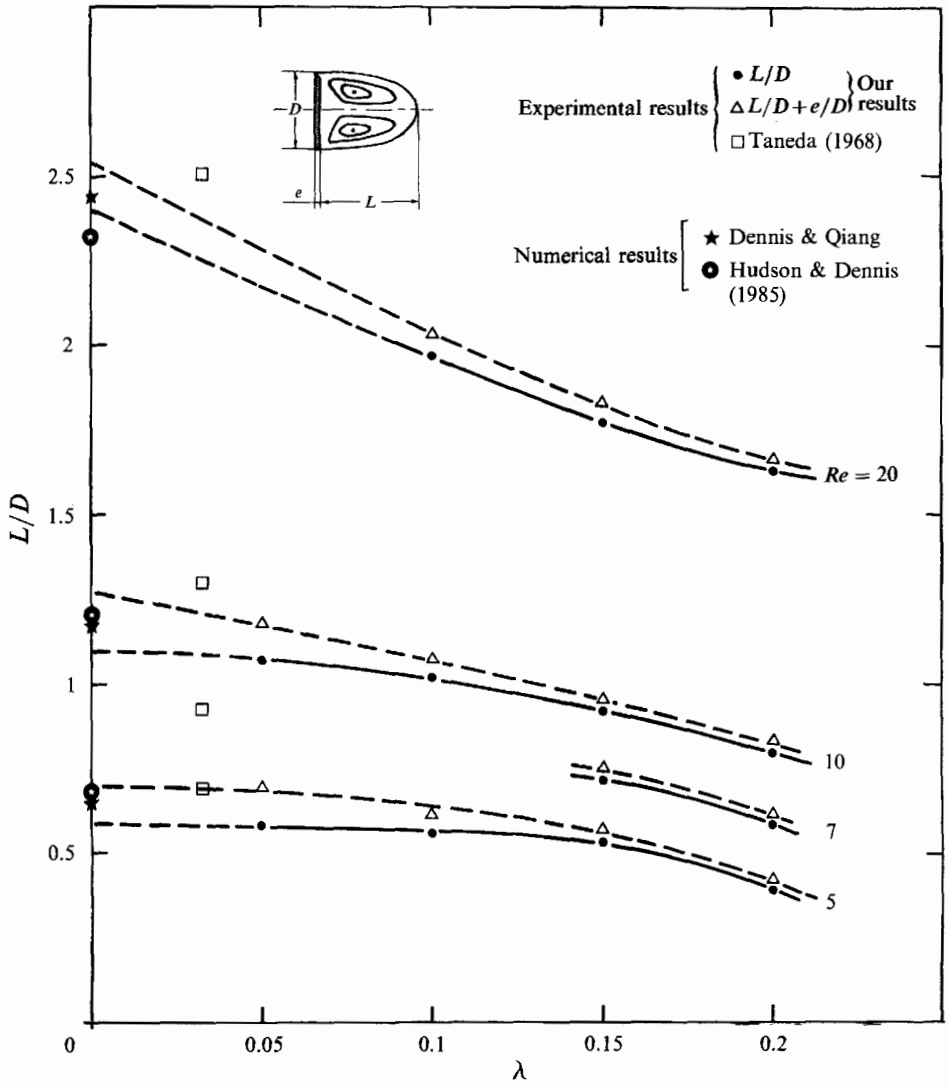

FIGURE 13. Limit of L/D as a function of λ.

and studied their evolution both as a function of the blockage ratio in the range $0.05 \leqslant \lambda \leqslant 0.2$ and of the Reynolds number in the range $5 \leqslant Re \leqslant 20$ for which the flow tends to a steady state; the experimental flow becomes unstable soon after $Re = 20$. The investigation of the steady-state properties of the wake as a function of λ has enabled us to deduce values of the characteristics of the flow for $\lambda = 0$ and thus to be able to make comparisons with the results provided by the numerical calculations for flow in an unbounded medium.

In the numerical part of the study, the present results generally confirm and supplement the previous calculations of Hudson & Dennis (1985) over the range $Re = 0.5$ to 20, which covers the range of the experimental study. There is good agreement between both sets of calculated results and the experiments but the calculations are not in accord with those of Ingham *et al.* (1990), probably owing to a blockage effect in their case of an infinite array of plates. The present calculations

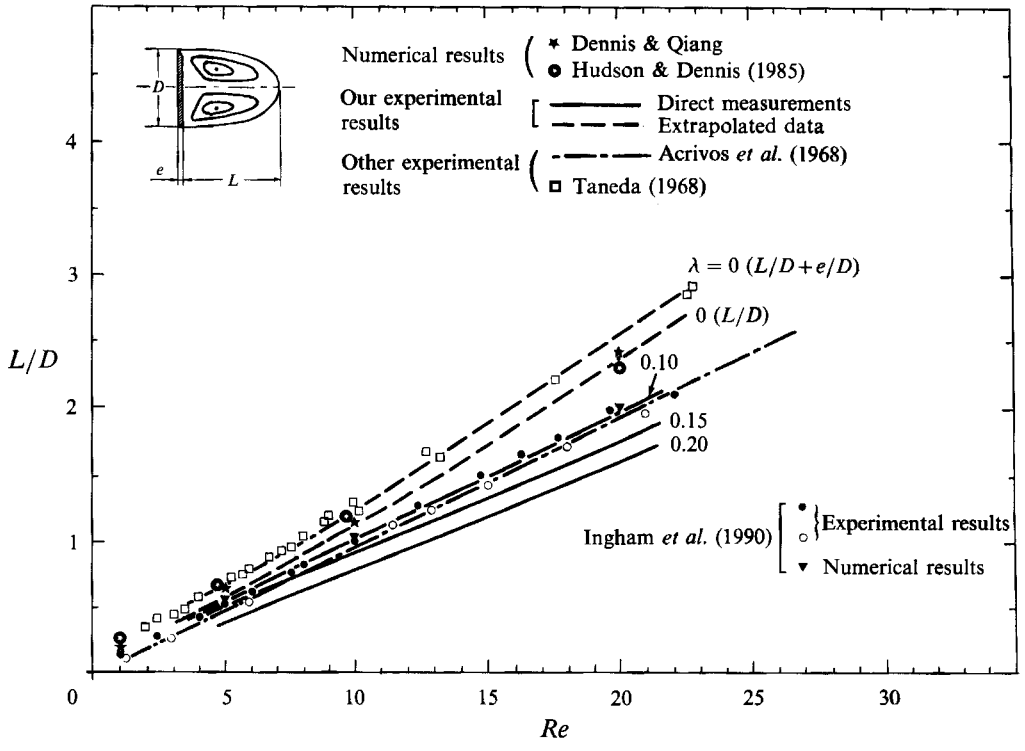

FIGURE 14. The length of the twin vortices plotted against Reynolds number.

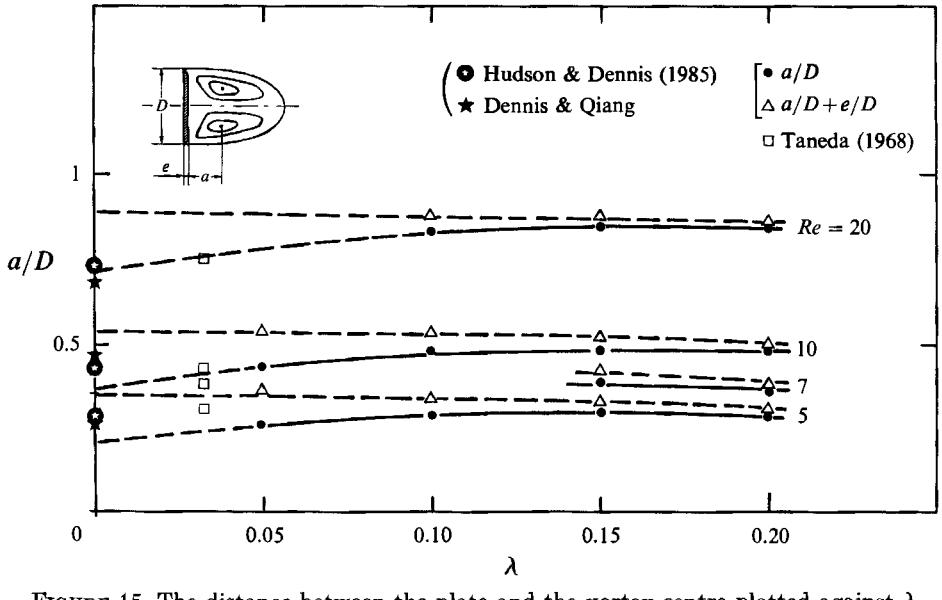

FIGURE 15. The distance between the plate and the vortex centre plotted against λ.

have been continued up to $Re = 100$ and the main properties of the wake have been scaled in table 4 according to the expected variations with Re discussed generally by Smith (1979, 1985), Peregrine (1985) and found in the numerical work of Fornberg (1980, 1985) for flow past a circular cylinder. The theoretical variations with Re for

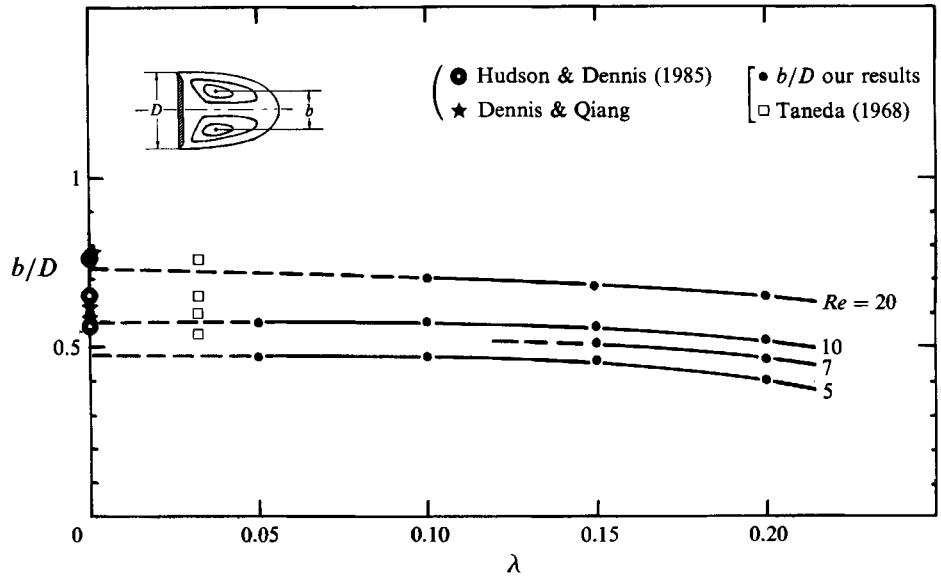

FIGURE 16. The distance between the two vortex centres plotted against λ.

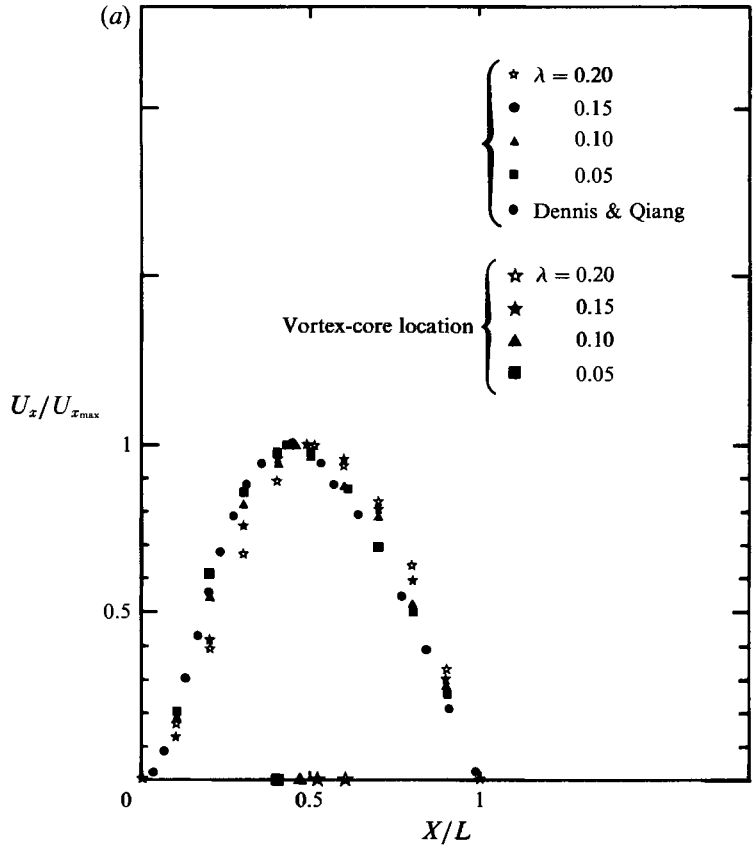

FIGURE 17(a). For caption see facing page.

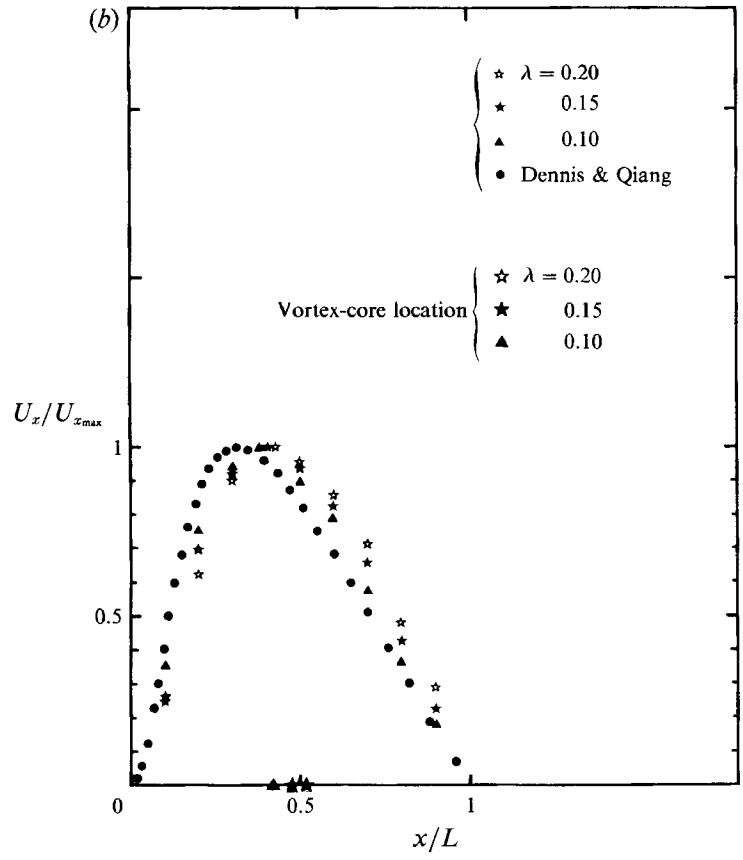

FIGURE 17. Dimensionless velocity profile along the recirculating bubble axis. (*a*) $Re = 10$. (*b*) $Re = 20$.

	Experimental ranges			Calculated		
				a/L		*b/d*
				Hudson & Dennis	Dennis & W-Qiang	Hudson & Dennis
Re	λ	*a/L*	*b/d*	($\lambda = 0$)	($\lambda = 0$)	($\lambda = 0$)
5	0.05–0.2	0.44–0.70	0.47–0.40	0.43	0.42	0.56
10	0.05–0.2	0.40–0.60	0.57–0.51	0.37	0.39	0.58
20	0.10–0.2	0.42–0.51	0.60–0.54	0.31	0.25	0.56

TABLE 6. Estimates of the location of the eddy core inside the wake bubble

the length and breadth of the wake seem to be reasonably well confirmed, although it is open to question as to whether numerical results in this range of *Re* can be justifiably compared with asymptotic results valid mainly as *Re* becomes large. However, the results of Ingham *et al.* (1990) for the array of plates give a linear variation of eddy length over the entire range of *Re* from 10 to 500 and with only a 5% deviation even at $Re = 5$. Nevertheless, the present results seem to give at least a coherent link between experiment and Navier–Stokes calculations and theory over the range of *Re* considered.

The present research has been supported by a grant from NSERC of Canada and also by grant no. 850416 of NATO. An early account of the numerical part of the investigation was presented by S.C.R.D. and W.Q. at the 29th British Theoretical Mechanics Colloquium at the University of Nottingham, UK, 1987 and some visualization comparisons were given by M.C., S.C.R.D., J.D.H. and J.-L.L. at the Flow Visualization Conference in Prague, Czechoslovakia, 1989.

REFERENCES

ACRIVOS, A., LEAL, L. G., SNOWDEN, D. D. & PAN, F. 1968 Further experiments on steady separated flows past bluff objects. *J. Fluid Mech.* **34**, 25.

ARAKAKI, G. 1968 The growth and development of the wake behind inclined flat plates at low Reynold numbers. *J. Sci. Hiroshima Univ.* Ser. A-II, **32** (2), 191.

BELOTSERKOVSKII, O. M., GUSHCHIN, V. A. & SHCHENNIKOV, V. V. 1975 Use of the splitting method to solve problems of the dynamics of a viscous fluid. *USSR Comput. Maths Math. Phys.* **15**, 190.

COUTANCEAU, M. & BOUARD, R. 1977*a* Experimental determination of the main features of the viscous flow in the wake of a circular cylinder in uniform translation. Part 1. Steady flow. *J. Fluid Mech.* **79**, 231.

COUTANCEAU, M. & BOUARD, R. 1997*b* Experimental determination of the main features of the viscous flow in the wake of a circular cylinder in uniform translation. Part 2. Unsteady flow. *J. Fluid Mech.* **79**, 257.

DENNIS, S. C. R. 1960 Finite differences associated with second-order differential equations. *Q. J. Mech. Appl. Maths* **13**, 487.

DENNIS, S. C. R. & CHANG, G.-Z. 1969 Numerical integration of the Navier–Stokes equations for steady two-dimensional flows. *Phys. Fluids* **12**, Suppl. II–88.

DENNIS, S. C. R. & CHANG, G.-Z. 1970 Numerical solutions for steady flow past a circular cylinder at Reynolds numbers up to 100. *J. Fluid Mech.* **42**, 471.

DENNIS, S. C. R. & HUDSON, J. D. 1978 A difference method for solving the Navier–Stokes equations. In *Proc. of the First Intl Conf. on Numerical Methods in Laminar and Turbulent Flow*, p. 69. London: Pentech Press.

DENNIS, S. C. R. & HUDSON, J. D. 1989 Compact h^4 finite-difference approximations to operators of Navier–Stokes type. *J. Comput. Phys.* **85**, 390.

DENNIS, S. C. R., HUDSON, J. D. & SMITH, N. 1968 Steady laminar forced convection from a circular cylinder at low Reynolds numbers. *Phys. Fluids* **11**, 933.

DENNIS, S. C. R. & QUARTAPELLE, L. 1989 Some uses of Green's theorem in solving the Navier–Stokes equations. *Intl J. Numer. Meth. Fluids* **9**, 871.

DENNIS, S. C. R. & SMITH, F. T. 1980 Steady flow through a channel with a symmetrical constriction in the form of a step. *Proc. R. Soc. Lond.* A **372**, 393.

FORNBERG, B. 1980 A numerical study of steady viscous flow past a circular cylinder. *J. Fluid Mech.* **98**, 819.

FORNBERG, B. 1985 Steady viscous flow past a circular cylinder up to Reynolds numbers 600. *J. Comput. Phys.* **61**, 297.

HARTREE, D. R. 1958 *Numerical Analysis*. Oxford: Clarendon.

HUDSON, J. D. & DENNIS, S. C. R. 1985 The flow of a viscous incompressible fluid past a normal flat plate at low and intermediate Reynolds numbers: the wake. *J. Fluid Mech.* **160**, 369.

IMAI, I. 1951 On the asymptotic behaviour of viscous fluid flow at a great distance from a cylindrical body, with special reference to Filon's paradox. *Proc. R. Soc. Lond.* A **208**, 487.

INGHAM, D. B., TANG, T. & MORTON, B. R. 1990 Steady two-dimensional flow through a row of normal flat plates. *J. Fluid Mech.* **210**, 281.

KAWAGUTI, M. 1953 Numerical solution of the Navier–Stokes equations for the flow around a circular cylinder at Reynolds number 40. *J. Phys. Soc. Japan* **8**, 747.

MAALOUF, A. & BOUARD, R. 1987 Étude de l'écoulement plan d'un fluide visqueux et

incompressible autour et au travers de coques cylindriques poreuses, à faibles nombres de Reynolds. *Z. angew Math. Phys.* **38**, 522.

OHMI, K., COUTANCEAU, M., TA PHUOC, L. & DULIEU, A. 1990 Vortex formation around an oscillating and translating airfoil at large incidences. *J. Fluid Mech.* **211**, 37.

PEREGRINE, D. H. 1985 A note on the steady high-Reynolds-number flow about a circular cylinder. *J. Fluid Mech.* **157**, 493.

PRANDTL, L. & TIETJENS, O. G. 1934 *Applied Hydro- and Aeromechanics*. McGraw-Hill.

SMITH, F. T. 1979 Laminar flow of an incompressible fluid past a bluff body: the separation reattachment, eddy properties and drag. *J. Fluid Mech.* **92**, 171.

SMITH, F. T. 1985 On large-scale eddy closure. *J. Math. Phys. Sci.* **19**, 1.

TANEDA, S. 1968 Standing twin-vortices behind a thin flat plate normal to the flow. *Rep. Res. Inst. Appl. Mech. Kyushu Univ.* **16** (54), 155.

TANEDA, S. & HONJI, H. 1971 Unsteady flow past a flat plate normal to the direction of motion. *J. Phys. Soc. Japan* **30** (1), 262.

WOODS, L. C. 1954 A note on the numerical solution of fourth order differential equations. *Aero. Q.* **5**, 176.